LUNDS UNIVERSITY

Wireless communication

EIT

MASTER THESIS

DESIGN, SIMULATIONS AND MEASUREMENT OF UWB ANTENNAS FOR WIRELESS BODY AREA NETWORK

AUTHOR:	Aida Garcia Lopez
AUTHOR:	Ernesto E. Lopez Canelon.
SUPERVISOR:	Rohit Chandra
EXAMINER:	Anders J. Johansson

7 SEPTEMBER 2012, LUND, SWEDEN

Abstract

Wireless Body Area Network (WBAN) is an emerging technology in the field of health monitoring. It consists of miniaturized sensors either wearable or implantable which communicate through a wireless link with each other or to a central device. The devices have to be ultra-low power. High data rate is also desirable. With the Ultra-Wideband (UWB) technology these requirements could be achieved. The antenna plays a vital role in these wireless devices. In this project two three-dimensional UWB antennas have been designed: a volcano antenna and a diabolo shaped antenna. The design and the simulations have been done on SEMCAD-X, which uses the FDTD method. A realistic numerical human phantom has been used to simulate the effect of the body, since the antenna will be placed on the body. These antennas are matched within the UWB range (3.1-10.6 GHz), with the S_{11} parameter below -10 dB. The volcano antenna (45x45x27 mm) has a bandwidth ratio of 3.9:1, and the diabolo shaped (17x17x15 mm) has a bandwidth ratio of 6.2:1. Both have omnidirectional radiation pattern for on-body communication. In addition, these antennas have perpendicular polarization with respect to the body surface, required for low loss of creeping waves, propagating over the body surface. The antennas were manufactured by 3D printing technology using steel, and then covered with copper tape to increase the conductivity and soldering ability to the connector. The measurement has been done with a Vector Network Analyzer for S_{11}, and the antennas were found to be matched in the UWB band. The path-gain (S_{21} parameter) between the volcano and diabolo antenna at 20 cm was measured with the VNA, resulting in an average parth-gain of -34 dB for co-polarization and -52 dB for cross-polarization, verifying the linear polarization of the antennas. This thesis confirms the hypothesis made by John D. Kraus of the volcano antenna and shows an alternative method of manufacturing antennas by 3D printing.

Foreword

We want to thank to all those who in a way or another have helped us to make this thesis. First of all to our coordinator Rohit Chandra whose time and knowledge were always at our disposition. To our examiner Anders Johansson, for his ideas and resources. To our international coordinator Maria Julia Fernandez Getino for her help and support during the whole year. To Ana Snachez Prieto, for helping us with the figures. To Marta Calvo, for the feedback. To Maria Isabel Hansson for giving us strengh in the presentation. And to all of you who have participated, thank you again.

- Gracias a mis padres, por darme todas las facilidades para lograr mis sueños. Nunca podré agradecéroslo lo suficiente. A Irene, porque te quiero más que a nada. A Sparta, habéis hecho que este año en Lund sea inolvidable. A todos los que, cerca o lejos, me habéis ayudado y apoyado. Y cómo no, a Ernesto, mi compi, por tantos ratos y tantos vídeos.

  Aída García.

- A mis padres, porque vuestro amor no tiene limites. Soy lo que soy gracias a vosotros. A mi hermana Lorena y mi hermano Rafa, porque han sido mi brújula cuando he estado perdido. A mi compi Aida, porque simplemente no se puede tener mejor compañera. A Maria Isabel, por estar siempre a mi lado y hacerme creer en la magia.

  Ernesto E. Lopez C.

Never give up on a dream. Just try to see the signs that leads you to it.

Paulo Coelho

Two antennas met on a roof, fell in love and got married. The wedding wasn't great but the reception was excellent.

Anonymous.

Contents

List of figures

Chapter 1

INTRODUCTION

The WBAN (Wireless body are network) is a relatively new technology that consists of low power and compact devices that communicate wirelessly between different parts of the body or with off body devices. This technology is very interesting for medical applications since it allows to transmit data between these devices, such as implants (pacemakers, hearing aids or sensors for monitoring temperature) or generic devices for presentation, storage and communication of data [1]. WBAN can offer numerous possibilities to improve health care and sports training facilities [2].

A very important part of the WBAN technology is the antenna used to recieve and transmit data. These antennas have specific features that make them different from other kind of antennas. In this case the antenna should be designed to have a small size since they are wearable or implantable. Depending on the application they might need a low directivity pattern (communication between the devices that are on the body either on the same side or the opposite side of the body). The antenna should also be able to overcome the effect of the human body's dielectric properties that will affect the matching properties of the antenna.For on body scenario, the antenna should be linearly polarized, and it should be placed with the electric field perpendicular to the body so the creeping waves travel over the surface. Low power radiation towards the body should be also achieved since the device will be close to the person. In some applications high data rate is also desirable. With the Ultra-Wideband (UWB) technology these requirements could be achieved with other inherit advantages of the UWB. Many researches have been made to develop UWB planar/microstrip antennas in the body area network since thay are easy to manufacture, low cost and can be very small. These antennas are not omnidirec-

tional and normally presents a directivity around 5-7 dB [3].Also, they can present an unstable radiation pattern that changes with frequency [4]. The purpose of this project is to design a UWB omnidirectional 3D small antenna that suits all the requirements explained above. The design and the simulation has been done with a commercial 3D electromagnetic solver, SEMCAD which uses the FDTD method. Since the antenna will be used on the body, the simulation has to be done taking the consideration of the human body. A 3D realistic numerical homogeneous human phantom has been used for this purpose. The measurements has been done with a Vector Network Analyzer.

In addition, a study of the UWB link loss channel have been done. First, a comparison with a narrowband WBAN model studied by LTH engineers [5] have been done in order to determine the adaptability of that link loss model in an ultra wideband scenario. Secondly, a quantitave study on a phantom cylinder of the path loss exponent is presented.

1.1 Structure of the report

This report is divided in 5 chapters:

- In Chapter I, the description of the problem is discussed.
- Chapter II is dedicated to explain the concepts needed to situate the area of research. First, an overview about ultra-wideband is presented. Then an introduction to ultra-wideband antennas is shown. Finally, focusing on our situation, ultrawide-band antennas on body networks are exposed.
- In Chapter III, the methodology used to find the solution to the problem is discussed. First a general scheme about the process followed to accomplish the task is presented. Afterwards, SEMCAD X, the program used to make the simulation, is introduced. Also a brief description of the FDTD method is given. Finally, the general settings used to run all the simulations of the antennas are listed.
- Chapter IV is dedicated to discuss the solution of the problem. Several possibilities to solve the problem are shown and two of them are chosen: the Volcano antenna and the Diabolo shaped antenna. These antennas are studied, simulated, fabricated and measured.
- Chapter V is dedicated to the study of the link loss model in a WBAN.

- In Chapter VI conclusions are presented.

1.2 Limitations

The majority of the existing UWB small commercial antennas are planar antennas that don´t fulfill the requirements of radiation properties within a broad bandwidth. The design of UWB three-dimensional small antennas is pretty new and few studies have been carried out. As a result, no empiric formulas are formulated in scientific papers or books, so it didn´t allow us to have an idea of the expected results. The design of the antennas became quite complex then. The final designs were got by approximations of trial and error and approximations with planar models. In addition, simulations took a lot of time due to problems with size, which slowed down the design process. Difficulties with the way of measuring the small antennas appeared, as a consequence of high cable effects introduced by the VNA connector. Although they were partially solved, some of them still persisted, so the results presented in this thesis could be used as a first approximation. Another limitation for this work is the lack of reliable S_{21} simulations, due to several problems with SEMCAD. No coherent results were shown when simulating in free space nor in the phantom case. For this reason, only the S_{11} parameter is explained in depth, with just a general view of the S_{21} behavior in free space in the VNA measurements.

With more time to develope this thesis, another antenna design would have been proposed. Also, another volcano and diabolo antennas would have been manufacture in order to measure the real S_{21} parameter between each pair. These measurements would have been done for free space and for on-body applications, with different positions along the body.

Despite these limitations, all the conclusion are robust enough to be able to verify the hypothesis made in the thesis.

1.3 Personal motivation

As telecommunication engineering students in Spain, we have always felt passion about wireless communication. After taking the Antenna Technology course in Lund University, we were exited to have discovered a different way of education, more simple and efficient than the one we were used to. All the team behind the course were capable of giving us full dosis of knowledge and motivation at the same time. We felt the wish to continue exploring the field of electromagnetic

theory focusing on antennas. In that way we had such an opportunity to improve our antenna knowledge by taking this thesis.

Chapter 2

RELATED CONCEPTS

2.1 History of UWB

As the electromagnetic spectrum is a limited resource, it needs to be efficiently exploited. Nowadays, this kind of applications is completely extended in all aspects of life, from military uses (long waves), mobile phones (radio), WiFi (microwave) to radiography (X-rays). So it is necessary to take full advantage of the spectrum to provide as much applications as possible.

The first experiments with short electromagnetic pulses were carried on in the late 1800s by using a spark-gap generator and arc discharges between carbon electrodes. Hertz's experiment in 1886 using two spark-gap generators, each one coupled with an antenna, proved the Maxwell's equations. Wireless communications were born. This was the first experiment to generate electromagnetic waves, and was the dominant technique for almost 20 years thereafter [6].

In the 1960s a new interest in UWB technology started again with the developing of new techniques for generating short pulses, the appearance of military radar improvements and the invention of the sampling oscilloscope, allowing its analysis in time-domain [7]. The invention of wideband radiating antenna elements, a short pulse receiver and the network analyzer in the 1970s contributed to the development of UWB technology, called by then 'baseband', 'carrier-free' communication or 'impulse radio'.

During the 1980s, this technology jumped from the military to the commercial sector. It was the U.S. Department of Defense who coined the term 'Ultra Wideband' in 1989, after 30 years of development and more than 50 patents in the field, covering transmitters, receivers, generators and radars [6], mainly through the work of H.F. Harmuth at Catholic University

of America, Ross and Robbins at Sperry Rand Corporation and Paul van Etten at the Air Development Center in Rome. In the 1990s, new components and a better understanding of the technology took UWB to a stage of maturity and to the opening to the commercial world, with high-performance, low-cost wireless communications sytems [8]. Another impediment in the commercial use of UWB was the fact that every country had assigned different narrow frequency band to specific services, interfering with UWB spectrum. It was in 2002 when the frequency regulator in the USA, the FCC (Federal Communications Commission), established the Report and Order for UWB to operate in the unlicensed spectrum between 3.1 GHz and 10.6 GHz, at limited transmit powers depending on the environments [7]. The aim was to minimize the interference with other applications, allowing coexistence with GPS, satellites, cellular systems, and others. As a result, scarce spectrum resources can be used more eficiently. In 2006, the Electronic Communications Committee (ECC) identified the conditions for the introduction in the European Union of radio applications based on ultra-wideband technology, and the mechanisms required to ensure protection of other radio services. This text, the 'ECC decision on harmonized conditions for devices using UWB technology in bands below 10.6 GHz', set the requirements for its development in Europe. It encourages the establishment of a single market where regulations are able to provide economies of scale [9].

The UWB market is continuously widing. Nowadays, UWB technology is applicable in all kinds of devices like computers, peripherals, mobile phones and domestic equipment due to its real mobility and its ease of installation [8]. Short-range high-speed communications tends to be the most popular application of UWB, with companies producing big volumes of UWB chips.

2.2 Theory

UWB is a short-range device (SRD) technology with a minimum bandwidth of 500 MHz or a fractional bandwidth (signal bandwidth/center frequency) of 20%. One of the main characteristics is the broad and flat power spectrum. With such a large bandwidth, very large spreading factors are allowed. As a result, very low power spectral densities are shown, generating a very low level of interference with other systems sharing the frequency range with Low Probability of Intercept (LPI) [8]. In these situations, any narrowband receiver will only detect the noise power within its own bandwidth, suppressing the interference by a factor similar to the spreading factor. In addition, this low radiation is almost undetectable for unauthorized listeners, and

enables the usage of long-life battery-operated devices. It must be seen that the spreading factor is a function of both the transmission bandwidth and data rate (SF=chip rate/symbol rate), so UWB systems with high data rates (>100 Mbits/s) have smaller spreading factors, being more sensitive to interference [7]. Moreover, this large bandwidth can lead to problems of accuracy in oscillators and timing circuits, due to a jitter of 1 ns in an application of 1 GHz of absolute bandwidth can cause horrible consequences [7].

Another important aspect of UWB is the high data rates achievable. As Shannon formula states, there is a trade between power and bandwidth. It calculates the capacity of a band-limited channel C (bps) in terms of channel bandwidth W (Hz), signal power S (Watts) and noise power spectral density No (Watts/Hz):

$$C = W \cdot log_2 \left(1 + \frac{S}{No}\right)$$

It shows that it is possible to have high capacity, hence high data-rates, by increasing the bandwidth even with low power. These high data-rates can be also traded for multipath performance. As a result, UWB can carry hundreds of megabits per second, much more than Bluetooth (2Mbps) and WiFi (54 Mbps) [10]. Another advantage of UWB technology is the short pulses that provide multipath immunity and robust performance by exploiting more resolvable paths [11].

The limits for the emitted power spectral density were set by the ECC in order to establish frequency masks and minimize the interference. There are some differences between the frequency masks in terms of indoor/outdoor environments, and wall and medical imaging, outside the UWB bandwidth [7], but within the bandwidth of interest, it remains -41.3 dBm/MHz.

UWB provides low-power and low-cost devices that can be very useful in positioning systems. The main applications of this technology are settled in the wireless communications field, but also in radar, imaging and sensing, like GPR, altimetry, security applications, logistics and medical applications.

In the last years, different UWB signalling schemes have been proposed. The two big groups where they can be settled are impulse radio (IR) as single-band option and OFDM as multiband one. The impulse radio sends very short duration pulses (ns or shorter), that are captured in the receiver by an extremely fast sampling oscilloscope. The excitation pulse bandwidth (on the order of GHz), which is determined by the duration of these pulses, must be much larger than

the antenna system bandwidth in order to obtain a good approximation of the system impulse response. The transmitted sequence is different for each user, according to a time-hopping (TH) code. This code solves the problem of spectral efficiency: even if a pulse collides with a pulse of other user, the rest of pulses will not, so the collisions are not catastrophic [7], [12], [13]. In the multiband case, the available spectrum is divided into several bands, each having a minimum of 500 MHz of bandwidth and OFDM. This scheme uses a multi-carrier modulation technique. Hence, the information is split into several low data-rate streams modullating diverse sub-carriers, and transmitting the data through parallel channels, making the symbol duration much larger than the delay spread. Subcarriers can overlap in frequency without ISI because each subcarrier spectral peak is at the nulls of their neighbourd carriers. OFDM is implemented by inverse fast Fourier transform (IFFT), reducing the complexity and cost of the system [13], [7], [12]. Comparing both alternatives, DS does not suffer Rayleigh fading (or very seldom), improving prime power and complexity without mitigation hardware. As a consequence, there is no need to forward error correction (FEC), so the power dissipation is much lower [14].

There are two more schemes for UWB. One of them is Direct Sequence (DS-CDMA), that spreads the signal by multiplying the original signal with a high-rate pseudo-random sequence, with a very large bandwidth. Usually, the spreading sequence consists of a sequence of 1s. Although IR and DS-CDMA have many similarities, the main difference is the nature of the spreading sequence. Meanwhile DS uses a bunch of 1s, IR consists of many zeros with several 1s located at random positions. The other approach to spread spectrum is frequency hopping (FH), where the carrier frequency changes several times during the transmission of a single symbol (fast FH) or one or several symbols are transmitted on the same frequency (slow FH) [7]. Some advantages of FH are the low probability of interference and the fact that the bandwidth of the frequency-hopping signal is determined by the available bandwidth, not by the rate of the FH sequence [12].

2.3 UWB antennas

The antenna plays a primary role in UWB systems. Considering the wide bandwidth UWB covers, the antenna design becomes essential. They must deal with bandwidth of impedance, mismatch, phase response, radiattion pattern, gain, polarization, return loss, some of them strongly dependent on the modulation scheme [15]. In addition, the size of the antenna is vital

for the design, mostly in the case of on-body applications, field where this technology becomes remarkably important.

Antennas are radiating elements that convert electric currents into radio waves, and vice versa. They radiate the electromagnetic energy of a transmission line to the free space, being considered as impedance transformers. In order to understand the challenges of designing an UWB antenna, several antenna parameters are listed below. Then, depending on the specific application they are designed for, the requirements will be optimized individually. Several antennas have been developed for UWB applications. The planar inverted-F antenna (PIFA) [16] is basically a microstrip patch antenna with a pin that reduces its size by half. By capacitive loading and low permittivity substrates, its narrowband can be enlarged. The simplified half finite circular tapered slot antenna with ground plane [10] with one blade is compared with others with multi circular blades. In this multi circular design it was shown a lower VSWR than a finite circular metal of similar size, and an improvement in bandwidth, efficiency and polarization integrity, achieving omni-directional patterns.

2.3.1 Antenna parameters

Impedance bandwidth

The impedance bandwidth is the frequency range within the antenna is correctly matched to its input transmission line. It can be defined in terms of the $|S_{11}|$ parameter, which level should be below -10dB, or in terms of voltage standing-wave ratio VSWR$<$2. These are obtained by the reflection coefficient τ, with τ = amplitude of the reflected wave/amplitude of the incident wave at the load. The perfect situation would be τ =0 indicating that no reflecting wave appears. On the contrary, this reflection in the load causes a travelling wave propagating down the transmission line to the generator [17]. Sometimes, if the cable is not long enough to attenuate that reflected wave, it reaches the generator and it is reflected back again to the antenna. As a result, it is partially transmitted into the channel. This effect is known as multiple signal reflection. A standard solution for this phenomena is to use a wideband resistive attenuator, an isolator or circulator between the generator and the antenna [6].

In UWB, due to the large bandwidth needed for transmitting information (7.5 GHz), the requirement of impedance bandwidth is really important and also complex to achieve.

Radiation pattern

According to IEEE, an antenna radiation pattern is defined as "a mathematical function or a geographical representation of the radiation properties of the antenna as a function of space coordinates". The power pattern is the representation of the spatial variation of the power density along a constant radius. Usually, the field and power patterns are normalized with respect to their maximum graph value (0dB) [18]. They are strongly dependent from the frequency, which means that different spectral components in a UWB signal will be radiated into different directions [19], [7]. Due to this issue, the design of UWB antennas becomes fairly tricky. Normally, radiation patterns are formed by several lobes, which are portions of the radiation pattern bounded by regions of relatively weak radiation intensity. For many on-body applications, it is desired that the main lobe embraces almost all directions, which is known as omnidirectional pattern. [18]

Gain

An isotropic radiator radiates the same amount of power in all directions, though it is not realizable in practice. The power gain G is the ratio of radiated power in a given direction relative to that of an isotropic radiator, radiating an amount of power equal to the power accepted by the antenna.

$$G = \frac{4\pi U(\theta, \phi)}{P_{in}}$$

Where $U(\theta, \phi)$ is the radiation intensity in the given direction and P_{in} is the power into losses antenna radiating uniformly in all directions [7], [19]. The gain of the antenna is one of the factors that affect to the calculation of the link loss.

Directivity

The directivity D is the ratio of the maximum radiation intensity U_{max} of the antenna to that of an isotropic radiator radiating the same amount of power [7].

$$D = 4\pi \frac{U_{max}}{P_{rad}}$$

It shows the maximum value of gain in a particular direction. For most cases in off-body applications, a high directivity is required since the external device can be fixed somewhere in the

room (e.g. the ceiling of a hospital room). On the other hand,for some on-body scenarios, it can be interesting to have a low directivity since the devices can be spread along the body.

Efficiency

It is the ratio between input power and radiated power. To calculate the efficiency of an antenna, reflection efficiency and radiation efficiency are considered. The reflection efficiency, or impedance mismatch efficiency, takes into consideration the reflective losses τ at the input terminals, expressed as $e_r = (1 - |\tau|^2)$. The radiation efficiency is the radiated power P to the total power P_{in} fed to the antenna, i.e. $e_{rad} = \frac{P_{rad}}{P_{in}}$. It considers the ohmic losses of the antenna through the dielectric material, and is determined in an anechoic chamber by several measurements [7], [20]. In WBAN, the most significant one is the radiation efficiency, due to the absorption by the surrounding tissues. Its efficiency can be severely reduced by the proximity of lossy materials [16].

Polarization

The polarization describes the orientation of the electric field at a specific position. In far-field, E-waves and H-waves oscillate in perpendicular planes. By a cut plane orthogonal to the direction of propagation, the kind of polarization can be seen. If the E_θ oscillates on a straight line, it is known as linear polarization. If two orthogonal dipoles are fed with currents in quadrature phase (shifted 90^o), then the E-fields would be circularly polarized [7]. For on-body aplications, it is required to have a linear polarization since the creeping waves over the surface suffer less attenuation than the penetrating waves.

Matching

An antenna is matched when the radiated power delivered from the generator at a given frequency is maximized. This is done by tuning the impedance of the antenna. This procedure is performed for a specific frequency in narrowband applications. For UWB, the matching have to be done in all the frequency range (3.1 GHz-10.6 GHz). Since the matching procedure is different for every spectral component, the matching process for an UWB antenna is very challenging [7].

Signal distorsion

To indicate how well a pulse is transmitted, the group delay has to be taken into account. It is given by the derivative of the unwrapped phase of the antenna. It must be constant within the frequency range, which is achieved if the phase is linear along the range. Also gain variations should be relatively flat across the bandwidth to prevent signal distorsion [20].

2.4 WBAN

Nowadays, electronics are desired to be present everywhere in order to improve our quality of life. One of the key applications of UWB technology is the medical systems, through a WBAN. A WBAN (Wireless Body Area Network) is a sensor network that connects various medical sensors, operating autonomously. They sense biological information and transmit it over a short distance. These sensors can be placed inside the human body (implants) or in close proximity (as in belts or pockets). They may be connected with a body central unit worn at the human body, or with another device close to it, as used in room hospitals. Also, this communication network could be a standard/mobile telephone network or a public WLAN hotspot (WiFi) [2].

A WBAN should be able to acquire periodic and non-periodic data sources, and transmit it to a external node within a fixed delay and without any loss, be reliable and self healing, and co-exist with other network devices without suffering any interference. This WBAN system offers two significant advantages compared to actual monitoring systems: mobility of the patient and independence of the location of the monitoring facility [2]. Currently, these networks are used to transmit and receive low data rate information (heart rate, blood pressure, etc), which requires low processing capabilities. But in near future, they can be needed to transmit high data rates (like video streaming), with the resultant powerful computational processing [7].

UWB provides solutions for the requirements of WBAN: high data rate transmissions, low probability of detention, low-power and longer battery life for body-worn units, essential for mobility. In recent years, the most popular wireless technologies for medical monitoring were ZigBee, WLAN, GSM and Bluetooth. Currently, UWB has joined that group. Comparing all these technologies, UWB is the one that has maximum data rate (up to 110 Mbps) comparing with WiFi (54 Mbps), Bluetooth (0.72 Mbps) and ZigBee (250 Kbps). It has the best coding efficiency (97.94%), the minimum transmission time (with a bit time of 9 ns), the minimum energy consumption (around the 7% of Bluetooth energy consumption), and therefore, the longest

battery life [21].

2.5 UWB antennas for WBAN

As described above, WBAN are specific applications where the antennas become especially important. Apart from all the requirements of low-power, large bandwidth and low returning losses, these antennas must be small. For body-worn WBAN scenarios, they need to be occult in the clothes for esthetic reasons. This is a very critical point because the smaller the antennas are, the worse properties they achieve. The shape of the antennas is also a very important issue. As it will be described below, a tiny change in a length or an angle may bring disastrous consequences of losses or radiation pattern.

Due to the electrical properties of the human body, movements of the person can lead to rapid changes in the communication channel behaviour. This is due to interactions of near field electric and magnetic fields with the body. The antenna parameters may therefore vary a lot: variations in antenna input impedance, shifts on resonant frequency and radiation pattern distraction. In addition, currents induced on body tissues produce significant losses in the system [16].

Several research have been done in on-body measurements of planar UWB antennas The compact planar monopole antenna [22] was measured in a homogeneous phantom and in a whole body model. It showed that S_{11} was slightly affected by the presence of the phantoms, achieving better performance than in free-space, but also showed a decrease in the gain. The best polarization was the perpendicular to the phantom. Results presented a bad performance when both antennas (transmitter and receiver) were located in opposite sides of the body (attenuation of 70 dB), but seemed achievable in directive links. All measurements confirmed the result of the simulations. The coupled planar dipole (CPD) [23] consists of a patch antenna combined with other two sided-coupled lines. The human body was simulated by a block of human muscle tissue. By the presence of human body, the gain decreased and the VSWR showed better performance. Measurements and simulations fitted very good. The planar inverted cone antenna (PICA) and the printed horn shaped self-complementary antenna (HSCA) were measured and compared in [24]. The PICA is derived from the volcano antenna and the circular disk antenna concepts. It showed good impedance bandwidth (8:1) and a gain of 3 to 6 dBi. The HSCA provided a better impedance bandwidth (10:1) and a gain of 0 to 2.4 dBi in the UWB band. Comparing their radiation patterns, the PICA showed a better one. When measuring on the human body, PICA

was placed perpendicular to the body and HSCA parallel. PICA presented stronger echoes and ringing effects due to its narrower bandwidth and the larger amount of resonance frequencies.

The butterfly antenna [25] was measured in the frequency band 1 GHz to 5 GHz. The radiation patterns were measured in free space, showing a dipole-like behavior, and in three body locations: head, chest and torso. The gain suffered slight variations in free-space and in the head, but great decrease up to -40 dB on chest and torso scenarios. The blockage caused by the body was critic in the back radiation in both E and H planes, increasing with frequency. It also depends on the antenna polarization.

Chapter 3

METHODOLOGY

In this chapter, the process of design followed to make this project is discussed. Also a brief overview of the program used to make all the analysis of the antennas, SEMCAD X is introduced. After that, a short description of the FDTD method is presented. Finally, the common settings used in SEMCAD to simulate are explained in case further checkout is needed.

3.1 Process of Design

Once an initial idea for the design has come up with, it is modeled in 3D and simulated in SEMCAD. This simulation will give us an approximate understanding of its behavior, showing the near-field, far-field and measures of losses, current, voltage, power, impedance and SWR (Standing Wave Ratio). Secondly, the design is improved in order to get a better VSWR, radiation pattern and smaller size. After that, the design is sent to manufacture. The company in charge of this procedure is Shapeways [26], a spin-out of Royal Philips Electronics. It is a 3D printing business headquartered in New York, with offices in Eindhoven and Seattle. They provide a platform where the user can upload his own design, which will be then manufactured and sent to the user. There are several materials to be chosen such as plastic, glass and metal, with different types each. Stainless steel and silver were the metals available, so the antennas developed here will be made of stainless steel, with bronze infused. The technical properties of this 3D printed stainless steel are shown in the following link [26]. The process that has been followed to design the antenna is shown in the figure 3.1.

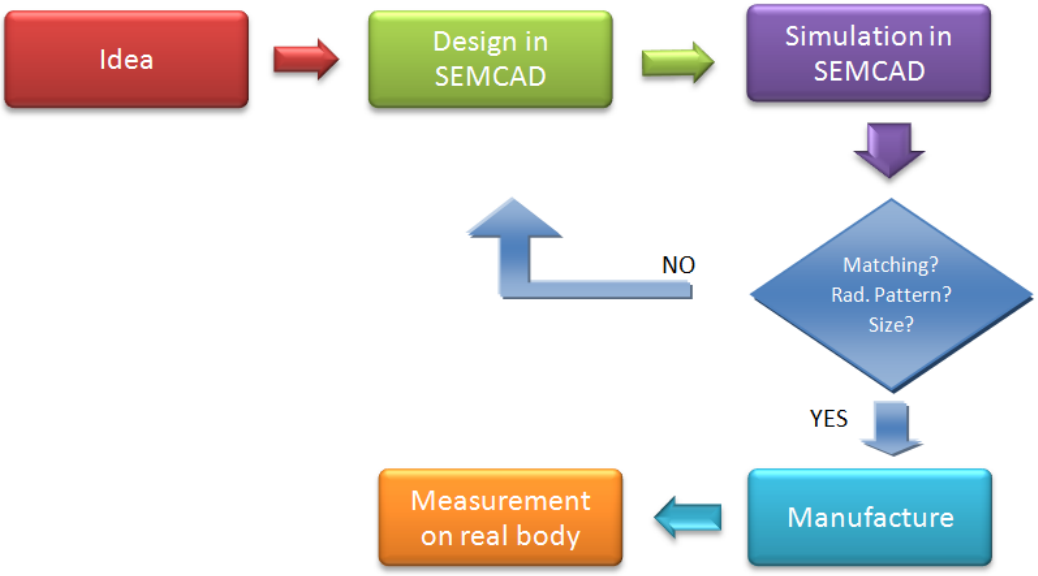

Figure 3.1: *Process flowgraph.*

3.2 SEMCAD

To measure and simulate the antennas, the software SEMCAD-X has been used [27]. SEMCAD (Simulation Platform for ElectroMagnetics Compatibility, Antenna Design and Dosimetry) is a powerful TCAD (Technology Computer Aided Design) tool for the analysis, design and optimization of antennas developed by SPEAG (Schmid & Partner Engineering AG).It was first released in December 2000, and after several versions, the actual one which has been used in this thesis is the SEMCAD X 14.6. It is a 3-D full wave simulation platform based on the FDTD and FEM method that provides RF and low frequency solvers, addressing the electromagnetic needs for several applications such as wireless, medical, EMC, dosimetry, microwave, thermal and optics. Some characteristics that SEMCAD offers are PEC/dielectric conformal modeler, multiport simulations, high performance UPML ABCs (Uniaxial Perfectly Matched Layer, Absorbing Boundary Conditions), postProcessing interface, a Python scripter and an optional hardware accelerated FDTD (aXware kernel) that can reduce runtime by 10 times. In addition, it includes several anatomical inhomogeneous high-resolutions human and animal models, including phantoms for children, adult men and women. SEMCAD is the most efficient tool for antenna design and simulation of the market, setting new standards in CEM software [27].

3.3 FDTD

The Finite-difference time-domain (FDTD) method is the easiest and most powerful engineering tool to calculate electromagnetic simulations. This full-wave technique was first introduced by Kane Yee in 1966 and further developed by Taflove in 1970s [28]. It applies second-order central differences as approximation to spatial and temporal derivatives that appear in Maxwell's equations (3.1).

$$\begin{aligned} \vec{\nabla} \cdot \vec{E} &= \frac{\rho}{\epsilon_0} \\ \vec{\nabla} \cdot \vec{B} &= 0 \\ \vec{\nabla} \times \vec{E} &= -\frac{\vec{\partial B}}{\partial t} \\ \vec{\nabla} \times \vec{B} &= -\mu_0 \vec{J} + \mu_0 \epsilon_0 \frac{\vec{\partial E}}{\partial t} \end{aligned} \tag{3.1}$$

After discretizing the domain in N cells (voxels), Maxwell equations are evaluated in each cell. Electric and magnetic fields are evaluated one time-step into the future, so that all the cells are solved [29]. This method can simulate all wave effects such as propagation, scattering, diffraction, reflection and polarizations, and can also model anisotropy, dispersion and other nonlinearities [30] which makes it usefull to use in WBAN scenarios.

3.4 Settings for the simulation

A model can be formed by points, curves, surfaces and solids. There are some standard shapes like circle, sphere, brick, cone and cylinder used to develop the designs. It also provides tools such as move, rotate, unite, subtract and sweep around and axis, very useful for the designer. Once the model is assembled, the characteristics of the simulation must be settled. There are two possible excitation modes, harmonic and broadband. In the harmonic one, a sinusoidal waveform is used as excitation of the simulation; in the broadband one, a Gaussian sine waveform is used. In this project, the broadband excitation will be used due to the wide bandwidth (3.1 GHz to 10.6 GHz) of UWB. The center frequency will be 6.85 GHz with a bandwidth of 7.5 GHz. The simulation time will be set as 10 periods, where a period represents the duration of the simulation excitation waveform which will be defined by the center frequency. The extracted frequency label shows the frequencies that could be shown in the results. All the figures will be set at the center frequency

6.85 GHz. The solver used is FDTD. The rest of labels are settled by default. Secondly, the type of region is chosen. All of the models will be PEC/Metal, except the phantoms that will be dielectric with the respective permittivity and conductivity. As the antennas are composed by perfect conductors (PEC), there would be no losses (no Lossy Metal, no Thin Resistive Sheet). The type of source used in this project will be an edge source, which simulates the coaxial cable connector used in the measurements. It is a voltage source with 50 Ω resistance. When placing the sources, the necessary sensors are automatically set: far field, overall field and sensor of edge source. They will show the radiation pattern, electromagnetic data ($\vec{E}, \vec{H}, \vec{D}, \vec{J}$), losses and many other parameters. No lumped elements will be used in this project. The boundaries are automatically settled, with ABC type (infinite domain), UPML/CPML (Convolutional PML) mode and medium absorption strength in all sides.

After setting all these parameters, the voxels are made. It is necessary to view the voxels in order to make sure that cells of the ground plane should not touch the top part, otherwise a short circuit will be produced and the simulation will be mistaken. Finally, the simulation is run.

Once the simulations in free space meet the requirements of bandwidth (3.1 - 10.6 GHz) and matching (below -10 dB in all the bandwidth), simulations with a homogeneous phantom are run. Permittivity (ϵ_r) and conductivity (σ) for dry skin are set for different frequencies. For the low-cutoff frequency (3.1 GHz) these turn to be ϵ_r =37.358 and σ = 1.7949 S/m; for the center frequency (6.85 GHz) are ϵ_r =34.22 and σ = 4.67 S/m; and for the high-cutoff frequency (10.6 GHz) are ϵ_r =30.705 and σ = 8.7019 S/m [31].

Two different designs were developed in this project: a volcano antenna with wave ground plane and a diabolo-shape antenna. All of them will be explained in detail.

Chapter 4

ANTENNA DESIGN

For UWB systems, a great amount of antennas have been studied in order to perform good characteristics along the wide range. They can be classified by following different standards, such as radiation pattern (omnidirectional vs directional antennas), frequency dependence, shape and size. Examples of omnidirectional antennas are planar-dipole and slot antenna in 2D, and biconical and discone antennas for 3D. As directional antennas, the options are Vivaldi antenna, log periodic, tapered slot and spiral antennas for 2D; in 3D the available antennas are for example the TEM horn antenna and the reflector antenna.

As mentioned above, UWB antennas should be omnidirectional, and preferably frequency-independent, so that no matter the part of spectrum an application needs to use, its behavior would not vary. The Rumsey's principle is a very important theory that suggests that the impedance and pattern characteristics will be frequency independent if the antenna shape is specified just in terms of angles. This theory has been verified in spiral antennas and some log periodic antennas. However, these frequency-independent antennas don't fulfill the size requirement. Since WBAN systems are meant to be for body applications, the antennas should be small size. As a result, compact planar antennas, such as bow tie, diamond, circular and elliptical disc poles, have been studied in the last years. Planar monopoles antennas have been deeply studied. Moreover, planar slot antennas have tried to enhance the low-cut frequency and the rejection capability [7].

These planar antennas don't fulfill the requirements of stability of the radiation pattern along the frequency range and they not offer an omnidirectional radiation pattern. For this reason, 3D antennas have been developed: volcano antenna and a diabolo shaped antenna.

4.1 VOLCANO ANTENNA

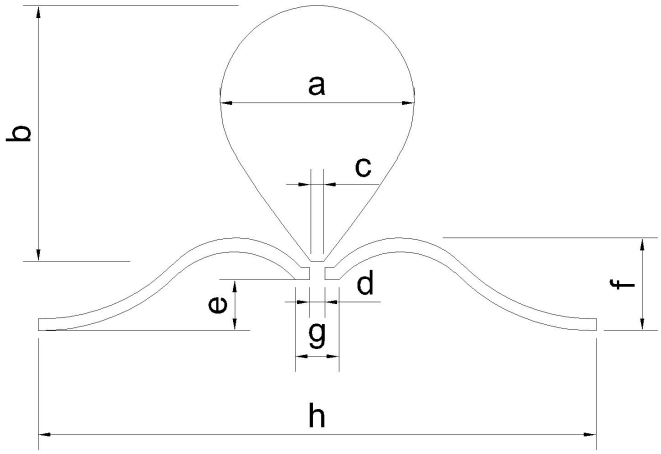

Figure 4.1: *Volcano Antenna Dimensions*

An omnidirectional frequency-independent antenna able to meet the low VSWR requirement was desired. Other antennas already developed, like double-ridged waveguide horn or log-periodic, didn't get them simultaneously. As the biconical antenna met all the requirements, it was taken as starting point. By replacing one of the cones with a finite ground plane, a discone was gotten, but it didn't fulfill the frequency-independent requirement. As a result, the volcano antenna was the next step to check [32]. This antenna was first proposed by Kraus [33], but no equations or parameters were done. Many research have been done with planar volcano antennas [32] [34] [35]. In this project, a 3D model half the size of the planar ones done before is achieved.

Starting with the figure shown in Kraus, the volcano antenna design is developed. By modifying step by step the shape and size of both the teardrop and the ground plane, an optimal model is obtained. It is composed by a cylinder cone and a sphere inscribed at the top.The ground plane was achieved by testing several dishes with different widths, heights and shapes. The final size results in a= 16 mm, b= 21 mm, c= 1.5 mm, d = 2 mm, e = 4.2 mm, f = 8mm, g = 3.5 mm, h = 45.6 mm as shown in 4.1. At the bottom of the cylinder cone there is a small hole of radius 1.6 mm that permits the connection to the feeding. The maximum height of the teardrop resulted to be around a quarter wavelength of the lowest operation frequency [32].

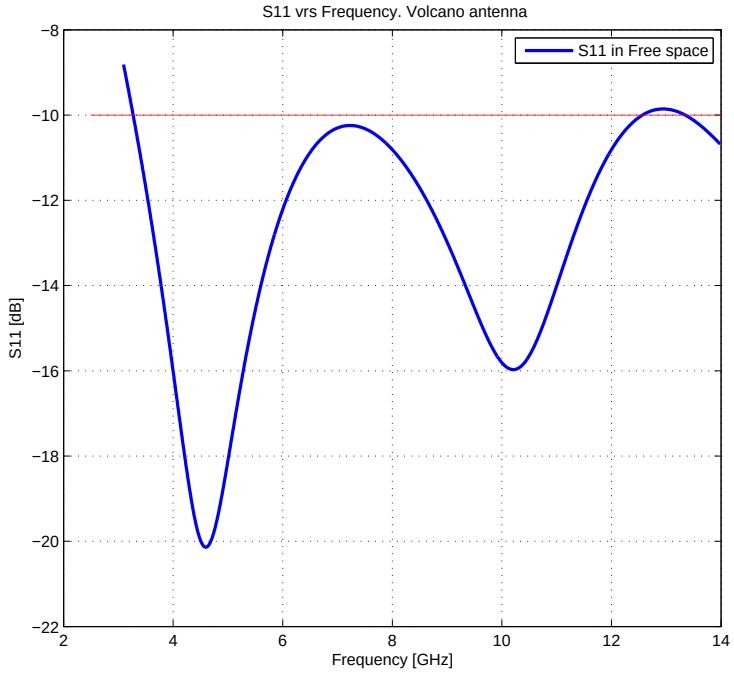

Figure 4.2: S_{11} *parameter for the Volcano antenna in free space.*

4.1.1 Simulations

The antenna was simulated in different environments in order to obtain its parameters. First of all, the antenna was situated in free space. Afterwards, a more realistic situation was set, by the usage of a homogeneous phantom that emulates the real human body.

Free space

The S_{11} parameter was simulated in order to observe the losses along the band. As figure 4.2 shows, in free space the low cutoff frequency is 3.2 GHz. Since the high cutoff frequency is 12.6 GHz, the bandwidth ratio results in 3.9:1 for VSWR<2.

A theoretical analytic method to calculate this low cutoff frequency is explained in [36]. In that case, the low cutoff frequency was computed over planar antennas, so in an attempt to adapt the method to this 3D case, the area of the teardrop will be calculated. Considering the height of our volcano antenna equal to the height of a cylindrical wire (l), it is possible to determine the f_c by equating the area of the teardrop to that of a cylindrical wire of height l and equivalent radius r given by $2\pi rl = S$. For real output impedance, the length of a cylindrical

monopole antenna is l = 0.24 x λ x F, where F =$\frac{l}{r}/(1+\frac{l}{r})$ So the resonant frequency is:

$$f = \left(\frac{c}{\lambda}\right) = \left(\frac{30 * 0.24}{l + r}\right) \tag{4.1}$$

where r and l are its radius and height. S is calculated by dividing the teardrop into a hemisphere and a truncated cone.

$$\begin{aligned} A_{hemisphere} &= 2\pi \cdot (a/2)^2 \\ A_{truncatedcone} &= \pi \cdot \left[m\,(a/2 + c/2) + (a/2)^2 + (c/2)^2\right] \end{aligned} \tag{4.2}$$

where m is the generatrix. Combining them, the area of the teardrop is:

$$A_{teardrop} = 2\pi \cdot (a/2)^2 + \pi \cdot \left[m\,(a/2 + c/2) + (a/2)^2 + (c/2)^2\right] \tag{4.3}$$

From figure 4.1 we calculate m = 1.49 cm, so the area of the teardrop results in S = 1.28π + 1.95π = 3.23π cm^2. Now, the equivalent r is obtained from S = 2πrl.

$$r = \frac{S}{2\pi l} = \frac{3.23\pi}{2\pi * 2.1} = 0.769cm \tag{4.4}$$

Now the low cutoff frequency can be calculated as $f_{c,theoretical}$ = 30*0.24/(l+r) = 7.2/(2.1+0.769)= 2.51 GHz. Since the real low cutoff is $f_{c,real}$ = 3.23 GHz, it is shown that the error between $f_{c,theoretical}$ and $f_{c,real}$ is 28.7 %.

Several simulations were made in order to prove the optimal design chosen. Changes in the size of the volcano antenna were carried out, including high and width of both the radiator element and the ground plane. Results are shown in the following figures, which indicate the properties of this antenna.

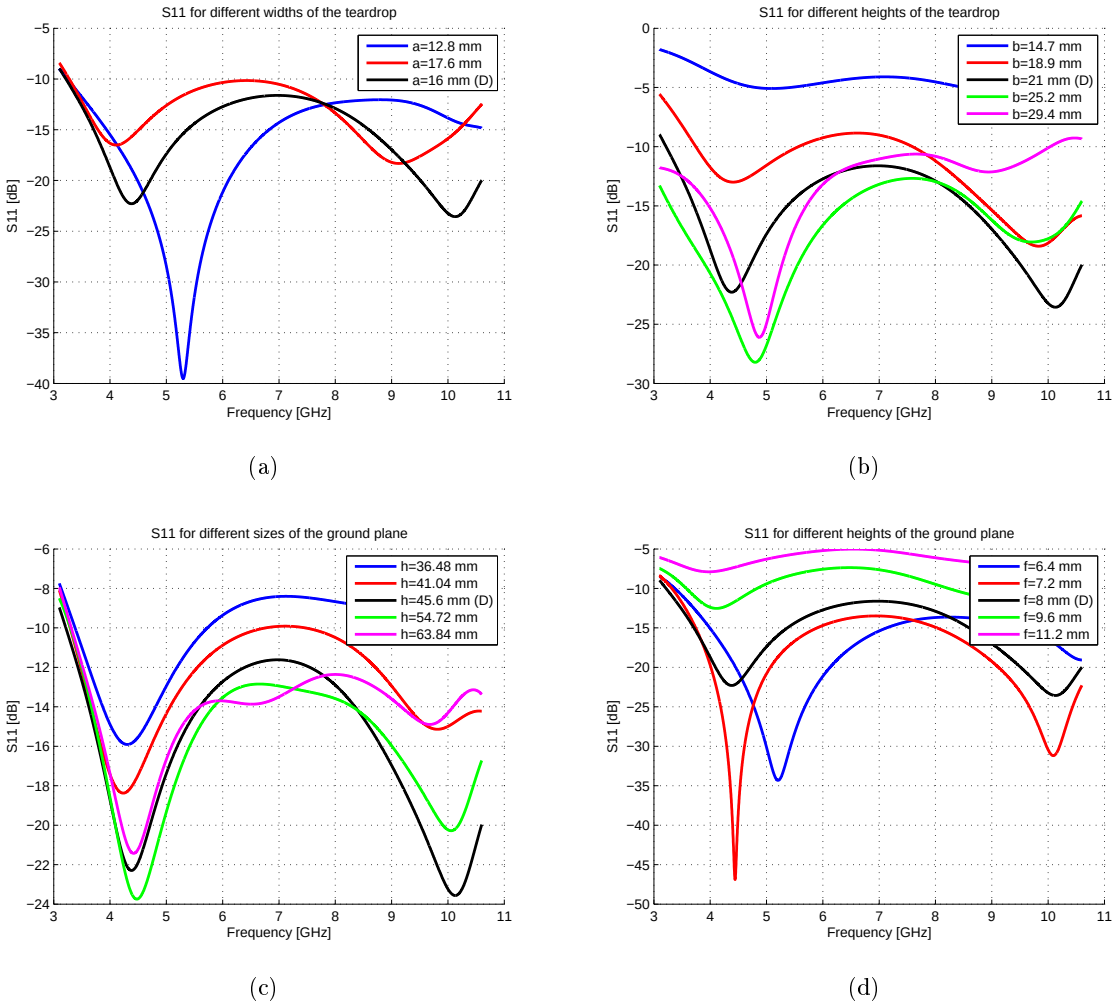

Figure 4.3: S_{11} **parameter for different changes in size of the antenna.** One parameters is changed while the others remain constant. (D) indicates the chosen value.

In figure 4.3 (a) it is shown that the low cut-off frequency doesn´t vary significantly with different widths of the teardrop. The wider the **a** parameter is, the higher losses it has. Since the width of the antenna wasn´t as important as its height, the final size was set as a=16.7 mm, because there was a slightly improvement in the low cut-off frequency comparing with the option of a=12.8 mm. Referring to the height of the teardrop, this was the most critic aspect when designing the antenna. It needed to be as lower as possible so that it will have more applications from an esthetic point of view. It is shown in figure 4.3 (b) that the lower **b** is, the worse S_{11} it has. The chosen high of b=21 mm seemed acceptable for the low cut-off frequency. In figure 4.3 (c), different sizes for the plate are presented. It can be seen that the smallest size with a loss diagram below -10 dB was h=45.6 mm, achieving also the best low cut-off frequency. In addition, several shapes for the plate were tested, varying the depth of the valley, but always gradually widening the distance between both conductors near the feed point.

The **radiation patterns** for free space are presented in figure 4.4. It can be observed the omnidirectional behavior of the antenna through the perpendicular polarization (Theta, normal to the body) in the 360^{o}, which in addition is much higher than the horizontal one (Theta, paralel to the body). From this it is seen that the antenna has a linear polarization, which is one of the goals. The transmission will be held in the perpendicular polarization, with an average gain of 0 dBi at 3.1 GHz, -2 dBi at 10.6 GHz and 0 dBi at 6.85 GHz. This gain proves that the volcano antenna suffers from losses if it is compared with a dipole, which has a gain of 2.15 dBi. A 3D plot of the radiation pattern at the center frequency is plotted in figure 4.4 (d). It is easy to observe its omnidirectional behavior in XY plane, meanwhile no lobes are faced to the Z axis.

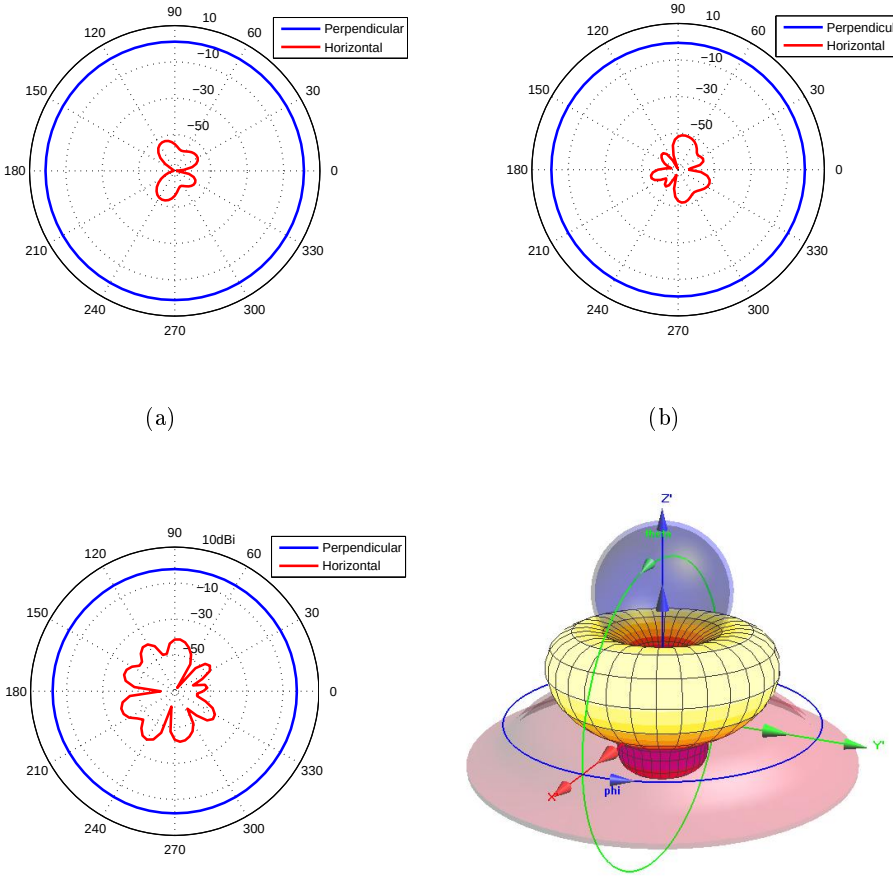

(a) (b)

(c) (d)

Figure 4.4: **Radiation Pattern of Volcano antenna in free space**. *(a) at 3.1 GHz.(b) at 6.85 GHz.(c) at 10.6 GHz. (d) at 6.85 GHz (3D).*

WBAN

Once all the parameters of the volcano antenna have been obtained in free space, it is necessary to simulate them on a real body. In order to do that, a homogeneous phantom representing the body is used, as figure 4.5 (a) shows. As the penetration depth for 6.85 GHz in skin is 0.0067477[m], it is assumed that the effect of the inner parts of the body will be negligible compared to the effect of the skin. Therefore , the parameters are set as if the dielectric properties of the whole body would be skin at the center frequency of 6.85 GHz, this is a permittivity of ϵ=34.22 and a conductivity of σ=4.67 S/m. The volcano antenna is placed in the back, where

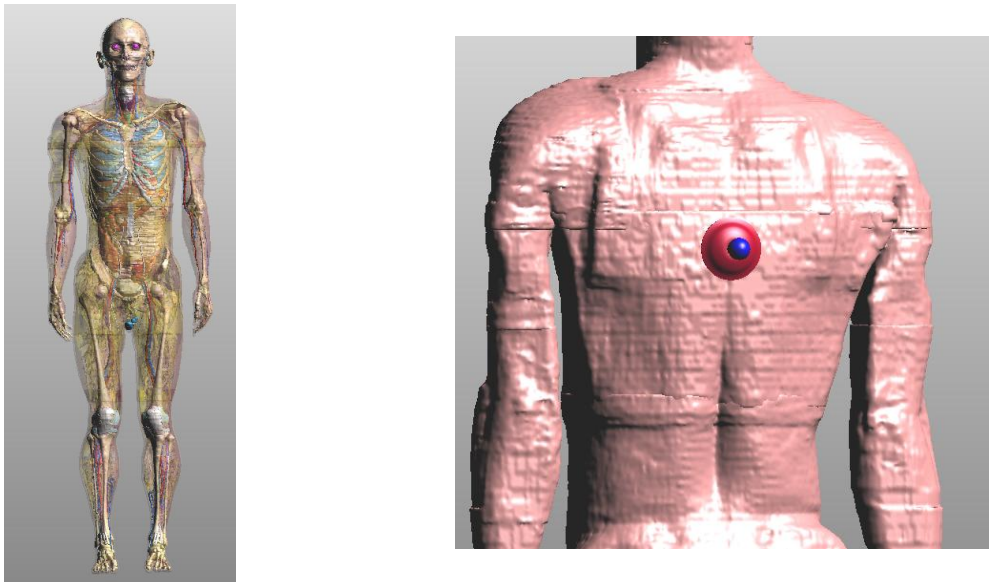

a) b)

Figure 4.5: **Homogeneous Human Body Phantom**. *(a) Front view. (b) Position of the antenna on the body.*

the surface is pretty flat as shown in figure 4.5 (b), resulting the S_{11} parameter displayed in figure 4.6. A comparison between the losses of the antenna in free space and with phantom is presented. It is observed that the phantom increases the losses in all the range, up to -9 dB. This effect is more visible at low and high frequencies (at 4.4 Ghz and at 10.1 GHz).

The **radiation patterns** for three different frequencies (3.1 GHz, 6.85 GHz and 10.6 GHz) in the presence of a homogeneous phantom are also presented in figure 4.7 and in figure 4.8 (a). Comparing with the free space case, it is noticed that no variation in the perpendicular polarization happens for 3.1 GHz and 6.85 GHz. Nevertheless, for 10.6 GHz, the diagram has become less omnidirectional, with slight differences in the gain, though always between -10 and 0 dBi. In contrast, the horizontal polarization has increased considerably, from -50 dBi in free space to -30 dBi in presence of phantom. Despite this increase, still the perpendicular polarization is the dominant, and will be the one used to transmit the information. The 3D radiation pattern is plotted in figure 4.8 (b), where the omnidirectional behavior is shown, while no lobe is oriented perpendicular to the body. This is very useful for on-body transmissions, where the transmitter and the receiver may be located in the shoulder and the waist, for instance. In this way, the transmission will be successful, reducing the radiation towards the inside of the body or away

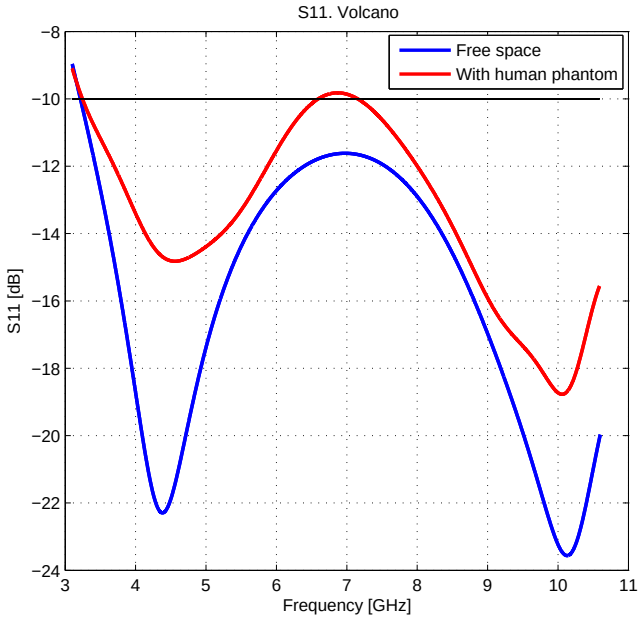

Figure 4.6: *S_{11} parameter for the volcano antenna in free space and in presence of a human phantom.*

from the body.

4.1.2 Measurement

To check the results of all the simulations made in SEMCAD, the S_{11} parameter was measured in the laboratory with the Vector Network Analyzer. Unfortunately, huge problems appeared in this phase. Since it is a small antenna, the size of the SMA connector became comparable with the size of the antenna, so great cable effects were displayed in the VNA, showing erroneous results. In addition, the material used to manufacture the antenna was not efficient enough. As the steel has a conductivity of $6.9 \cdot 10^{-7}$ S/m, the connection was not truly efficient. Also the steel do not get soldered properly to the tin, resulting in a very bad connection. In order to solve these problems, the antenna surface was covered with copper tape, both the radiating element and the ground plane. In addition, a thinner cable was soldered to the feeding point of the antenna, so that its effects were reduced. The final aspect of the antenna can be seen in figure 4.9 (b).

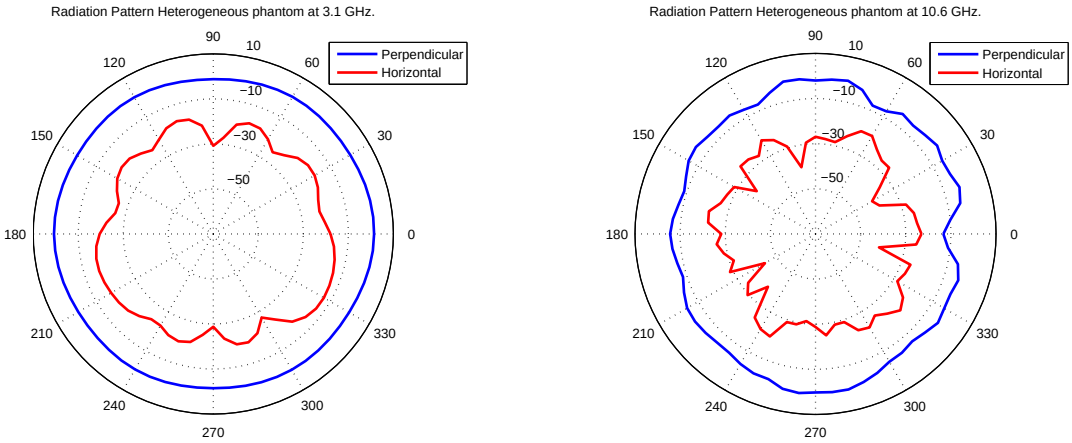

a) b)

Figure 4.7: **Radiation Pattern of Volcano antenna in presence of a homogeneous human phantom**. *(a) at 3.1 GHz. (b) at 10.6 GHz.*

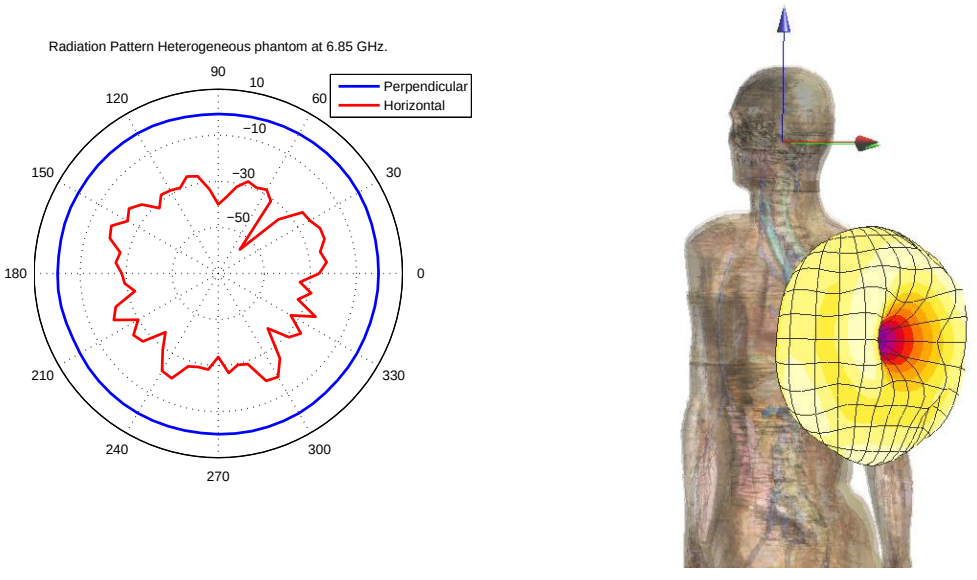

a) b)

Figure 4.8: **Radiation Pattern of Volcano antenna in presence of a homogeneous human phantom**. *(a) at 6.85 GHz. (b) at 6.85 GHz (3D).*

a) b)

Figure 4.9: Manufactured Antennas. *(a) Steel antenna SMA connector.(b) Antenna with copper surface and a thinner, 14 cm long connector.*

Once the problems were solved, the VNA obtained proper results. The VNA used in the measurements only displayed frequencies up to 8 GHz, so the last 2 GHz of the UWB range could not be measured. But the simulations showed a decrease of S_{11} from 7 GHz in both free space and with phantom, reaching the minimum in 10.1 GHz, so this limitation doesn´t seem so severe. As one can observe in figure 4.10 (a), the S_{11} parameter for free space is below -10 dB in all the range. The low-cutoff frequency is 3.16 GHz, almost the same as the extracted from the simulations which was 3.2 GHz. The minimum S_{11} is located around 4 GHz, as it was in the simulations. For the case of the human phantom, the measurements with the VNA were carried out in presence of the hands, placing them below the ground plane. In this case, the low-cutoff frequency is 3.11 GHz, almost the same as the simulated result, which was 3.2 GHz. In both cases, several peaks are observed,as a result of the cable effects, that couldn´t be completely removed. Even though, the losses seem to stay between -15 and -20 dB, with the on-body S_{11} above the free space one, which confirms the simulation results. The main difference between simulations and measurements happens in the range of 4-5 GHz. While lowest values achieved in the simulations reached -22 dB (free space) and -15 dB (phantom), the measurements show values of -50 dB (free space) and -32 dB (phantom). This change is explained as an error of the VNA in measuring such a small antenna, due to this impulsive behavior does not follow any

comprehensive explanation.

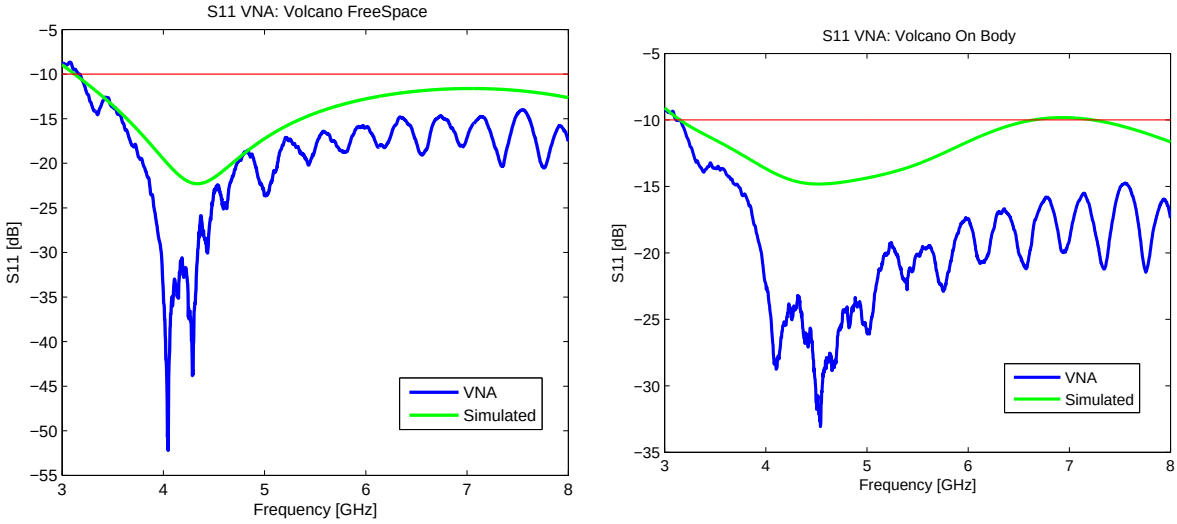

a) b)

Figure 4.10: S_{11} parameters measured in a VNA. *(a) Free Space.(b) On body (Hand).*

4.2 DIABOLO SHAPED ANTENNA

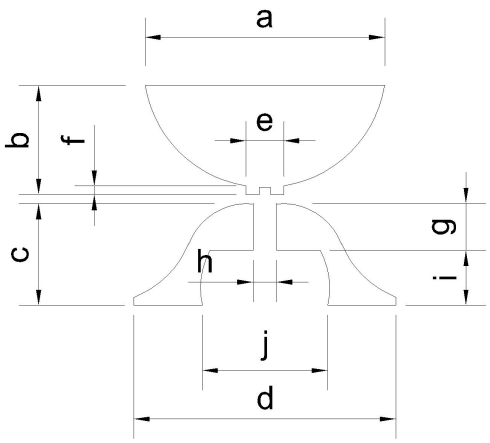

Figure 4.11: *Diabolo Antenna Dimensions*

This antenna has been designed by taking as inspiration the 3D biconical antenna and the 2D Vivaldi antenna. As the biconical antenna, it is formed by two opposing parts, a plate and an upper conductor. The feed is located between them. Instead of having straight lines, it has a smoothed shape like the Vivaldi antenna, having as a result a diabolo shaped antenna. A biconical antenna is theoretically capable of providing frequency-independent impedance if it has infinite length [7]. In a real scenario, the size has to be truncated since it is not possible to build infinite antennas, and this will also limit the bandwidth. The idea of making the antenna smoother is because going from abrupt transitions to more smooth-gradual ones results in wider bandwidths [33].Another reason is to make the current path in the antenna larger, increasing the radiation resistance. The polarization of this antenna is also linear, what makes it capable to be used in vertical polarization over the body, making the creeping wave to travel on the surface. The final design can be seen in figure 4.11. It is composed by a hemisphere with a spout as the radiating element, and a wave ground plane. The size of the antenna is : a = 15.3 mm, b = 7 mm, c = 6.5 mm, d = 16.7 mm, e = 2.4 mm, f = 1 mm, g = 3 mm, h = 1.8 mm, i = 3.5 mm, j = 7 mm and a gap between the conductors of 0.53 mm. The h and j parameters are set to adapt the antenna to an SMA connector.

4.2.1 Simulations

As in the case of the volcano, the diabolo antenna was simulated in free space and in a realistic environment by using a human phantom in order to obtain its parameters.

Free space

The S_{11} parameter gives details of the antenna behavior in terms of losses. As the figure 4.12 shows, the low cutoff frequency is 4.8 GHz. Since the high cutoff frequency is 29.8 GHz, the bandwidth ratio results in 6.2:1 for VSWR<2.The high losses in low frequencies (3.1 GHz) are caused by the high reflections of the radiation in the antenna. On the other hand, at 10.6 GHz, the waves have travelled along the whole radiating element, so higher radiation will be achieved, resulting in low losses, i.e. in low S_{11}.

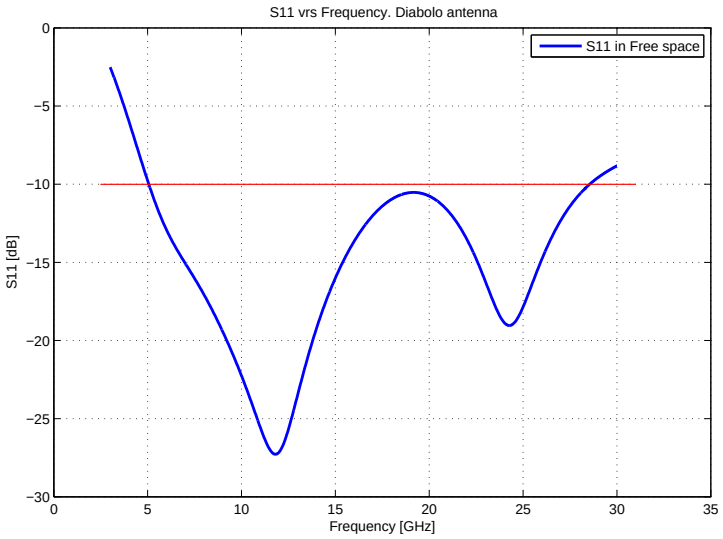

Figure 4.12: S_{11} *parameter for the Diabolo antenna in free space.*

As mentioned in the volcano antenna, there is a theoretical analytical method of calculating this low cutoff frequency [36]. In this case, the area of the upper conductor is easier to obtain. It can be approximated by the area of a hemisphere and the area of a circle. Considering the height of our antenna equal to the height of a cylindrical wire (l), the f_c is obtained. Since S = 2πrl, and computing l = 0.24 x λ x F, where F = $\frac{l}{r}/(1+\frac{l}{r})$, the resonant frequency is calculated with:

$$f = \left(\frac{c}{\lambda}\right) = \left(\frac{30 * 0.24}{l + r}\right)$$

where r and l are its radius and height. The area of the diabolo is:

$$A_{diabolo} = 2\pi \cdot (a/2)^2 + \pi(a/2)^2 = 3\pi(a/2)^2 \tag{4.5}$$

From figure 4.11 l = 0.7 cm, so the area results in S = 1.755π cm^2. The equivalent r is obtained, r = 1.25 cm.

Now the low cutoff frequency can be calculated as $f_{c,theoretical} = \frac{30*0.24}{l+r} = \frac{7.2}{0.7+1.25} = 3.69$ GHz

Since the real low cutoff is $f_{c,real} = 4.85$ GHz, it is shown that the error between $f_{c,theoretical}$ and $f_{c,real}$ is 31.5 %.

Here it can be observed that in both cases, volcano and diabolo, this error is approximately 30%, in contrast of the planar case studied in [36], where $f_{c,theoretical}$ and $f_{c,real}$ were almost the same.

Several simulations have been made in order to see how the different shapes affect the performance of the antenna. These changes induced variations in terms of losses, which were minimized so as the optimal design was achieved. The spout added in between the conductors presented an increase in the bandwidth of the antenna. The distance between the conductors was also an important factor showing that the higher the distance, the lower the matching.

In figure 4.13, different S_{11} of the Diabolo antenna are displayed for different sizes. These simulations have been done without the presence of a human phantom. These values have been chosen since the main problem is to get a good match at lower frequencies. As shown, the S_{11} remains below -10 dB for frequencies over 4.85 GHz. The **a** parameter was choosen to achieve the best lower frequency matching. The **b** and **c** parameters were choosen in order to achieve a compromise between size and bandwidth. It is seen that the higher the length of the antenna, the higher the bandwidth, but since miniaturization is required, the following values were chosen: a = 15.3 mm, b = 7 mm, c = 6.5 mm , d = 16.7 mm, f = 1mm and the gap was 0.53 mm.

In figure 4.13 it is seen that the value of **f** is not affecting the bandwidth significantly. Even though, the presence of a spout is increasing considerably the bandwidth [add f = 0 in the figure].

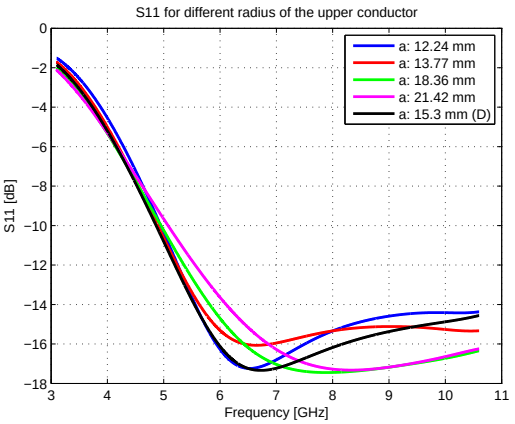

(a)

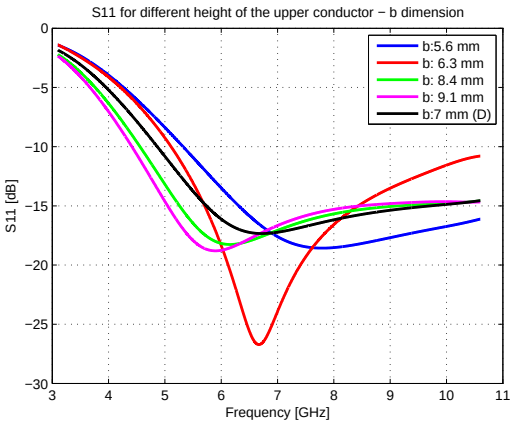

(b)

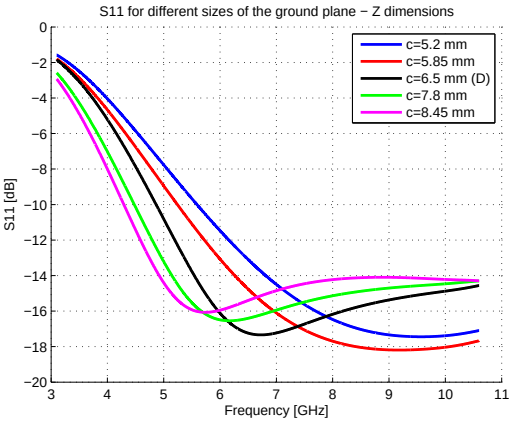

(c)

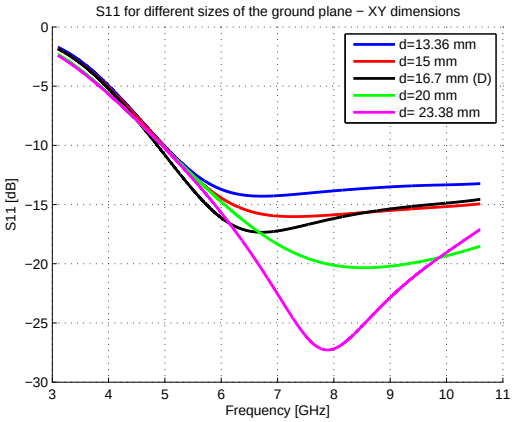

(d)

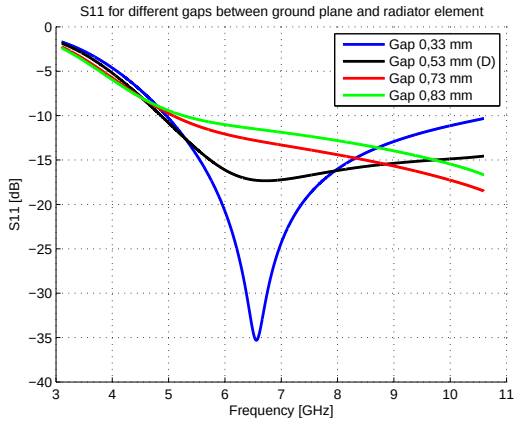

(e)

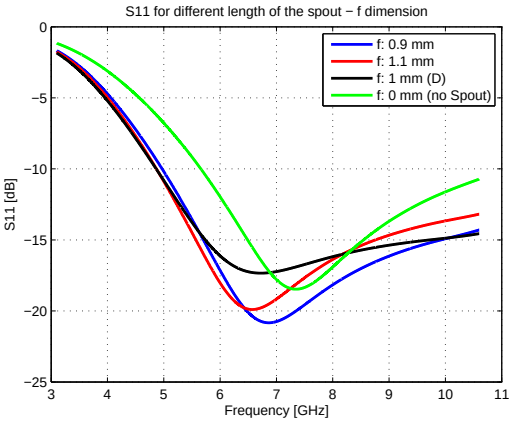

(f)

Figure 4.13: S_{11} **parameter for different changes in size of the antenna**. One parameter is changed while the others remain constant.(D) indicates the chosen value.

The **radiation patterns** for free space are presented in figure 4.14. It can be seen that in this case, the antenna is also omnidirectional in all the frequencies for the perpendicular polarization (Theta, normal to the body), meanwhile the horizontal polarization (Phi, paralel to the body) remains below -50 dBi. For this reason, the transmission will be held in the perpendicular polarization. The gain is constant in all the range, with a value of 0 dBi. A 3D plot of the radiation pattern at 6.85 GHz is shown in figure 4.14 (d), proving that it is omnidirectional in the XY plane, with no lobes in the Z axis.

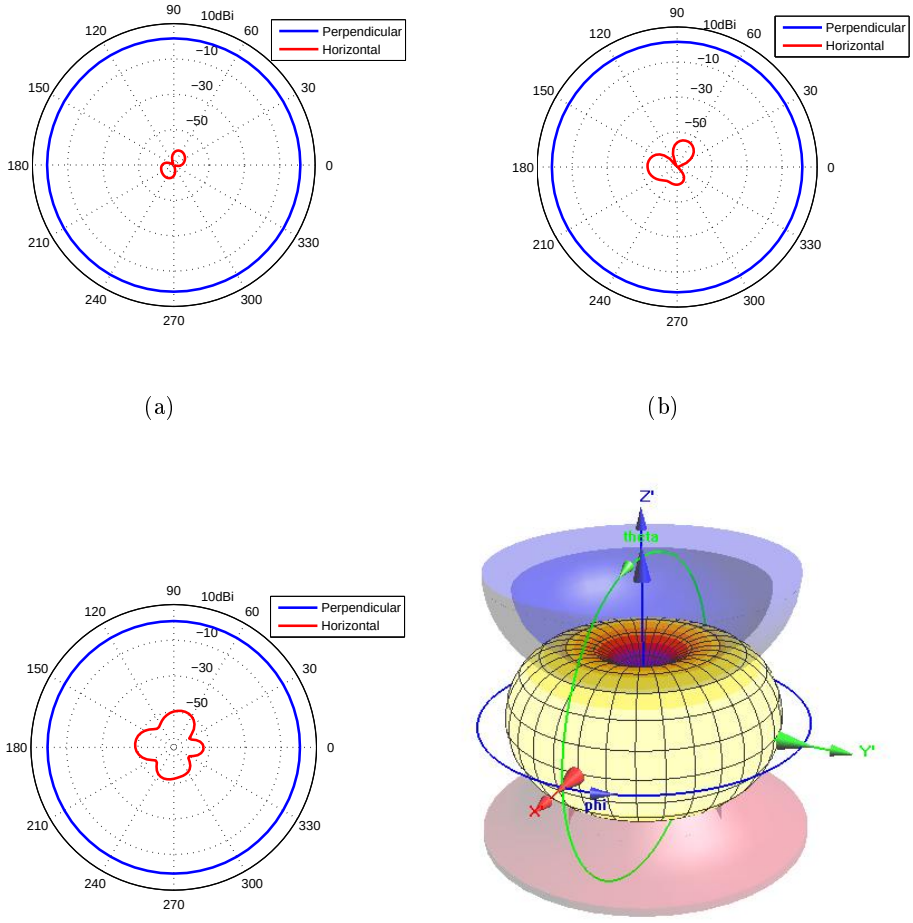

Figure 4.14: **Radiation Pattern of Diabolo antenna in free space**. *(a) at 6.85 GHz.(b) at 6.85 GHz.(c) at 10.6 GHz. (d) at 6.85 GHz (3D).*

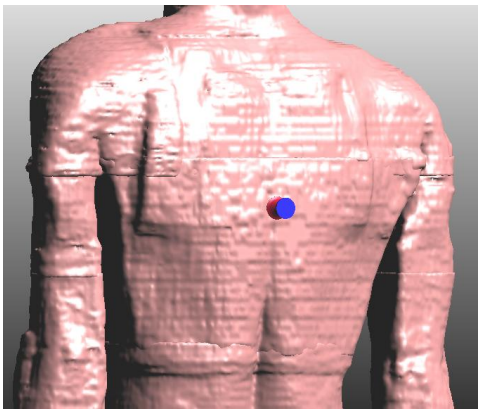

a)

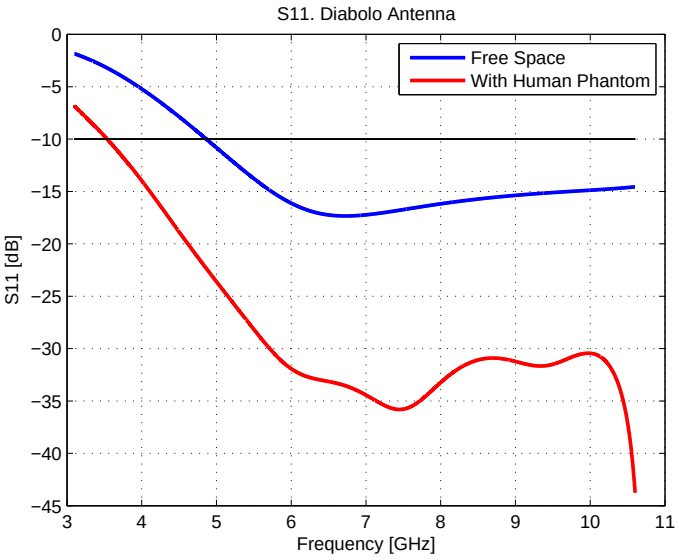

b)

Figure 4.15: S_{11} parameters in presence of a human phantom. *(a) Position of the antenna. (b)* S_{11} *graph.*

WBAN

The next step after observing the effects in free space is to simulate the behavior of the diabolo antenna in the body. In this way, the same phantom used with the volcano antenna is here used to obtain the S_{11}, with the skin properties at 6.85 GHz (ϵ=34.22, σ=4.67 S/m). For this, the diabolo antenna is placed in the back of the body, as shown in figure 4.15(a), resulting the S_{11} parameter presented in figure 4.15(b). It can be seen that the phantom have a big impact in the antenna matching. The S_{11} decrease in 15 dB within the whole UWB range, and the low-cutoff frequency in reduced almost 1.5 GHz, reaching 3.5 GHz. This is due to the effect of the body surface as a bigger ground plane.

The **radiation patterns** for different frequencies (3.1 GHz, 6.85 GHz and 10.6 GHz) in the presence of a homogeneous phantom are shown in 4.16 and 4.17 (a). Comparing with the free space case, the perpendicular polarization remains omnidirectional in the 360º, but with a slight decrease of the gain, which now is around -2 dBi. On the other hand, for horizontal polarization, the gain has increased up to -20 dBi, around 30 dB of difference comparing with the free space situation. Despite this change, the dominant polarization is still the perpendicular,

which will transmit the information. In 4.17 (b), the 3D radiation pattern is plotted, showing the omnidirectional behavior of the diabolo antenna.

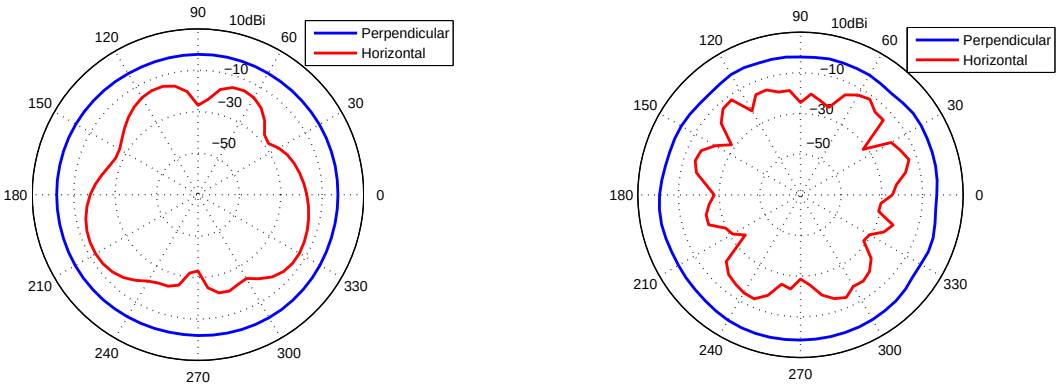

a) b)

Figure 4.16: **Radiation Pattern of Diabolo antenna in presence of an homogeneous human phantom**. *(a) at 3.1 GHz. (b) at 10.6 GHz.*

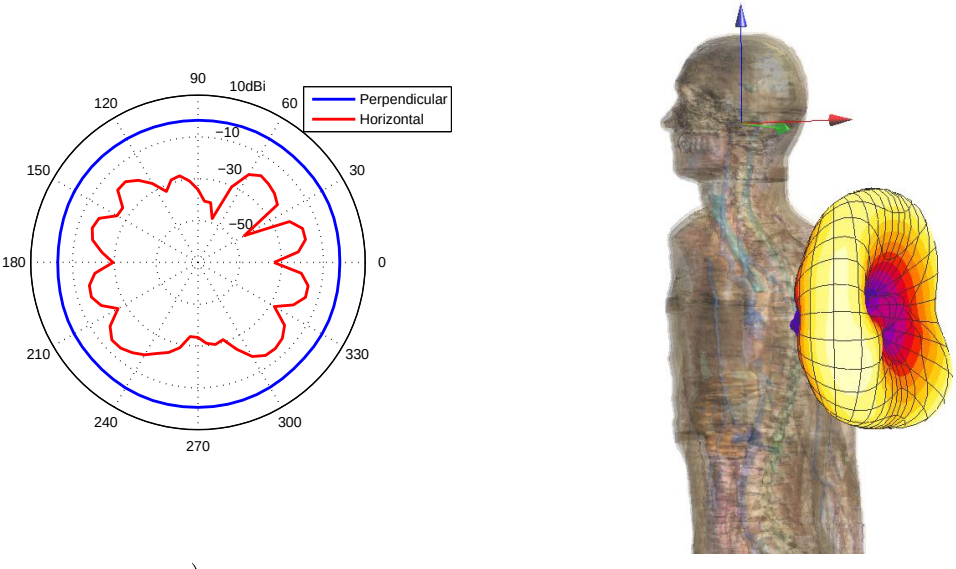

a) b)

Figure 4.17: **Radiation Pattern of Diabolo antenna in presence of an homogeneous human phantom**. *(a) at 6.85 GHz. (b) at 6.85 GHz (3D).*

4.2.2 Measurement

a) b)

Figure 4.18: Manufactured Antennas. *(a) Steel antenna SMA connector.(b) Antenna with copper surface and a 14 cm long and thinner connector.*

To check the result obtained through the simulations, the diabolo antenna was measured with the VNA. The same troubles with the steel and the cable effects explained in the volcano antenna section appeared in this case. They were solved by the same method of covering the antenna with copper and soldering a thin cable to the feeding point. The aspect of the diabolo antenna is displayed in figure 4.18 (b). Regarding the frequency range limitation (from 3 GHz to 8 GHz) of the VNA, the results are shown in figure 4.19. It is displayed that the low-cutoff frequency for free space is 5.2 GHz, and the S_{11} remains between -10 dB and -25 dB in the range 5 - 8 GHz, while the simulations showed a f_c of 4.8 GHz with a S_{11} in the range of -10 dB to -17 dB. For the on-body case, the hands were placed below the ground plane of the antenna. In this case, the S_{11} never reaches the -10 dB threshold, remaining in the interval -15 dB to -30 dB, meanwhile the simulations showed a f_c of 3.5 GHz, with a minimum value of S_{11} of -35 dB. It is derived that measurements accord with simulations. In both cases, the peaks observed in all the range are the result of the cable effects, that couldn't be removed completely, as mentioned before.

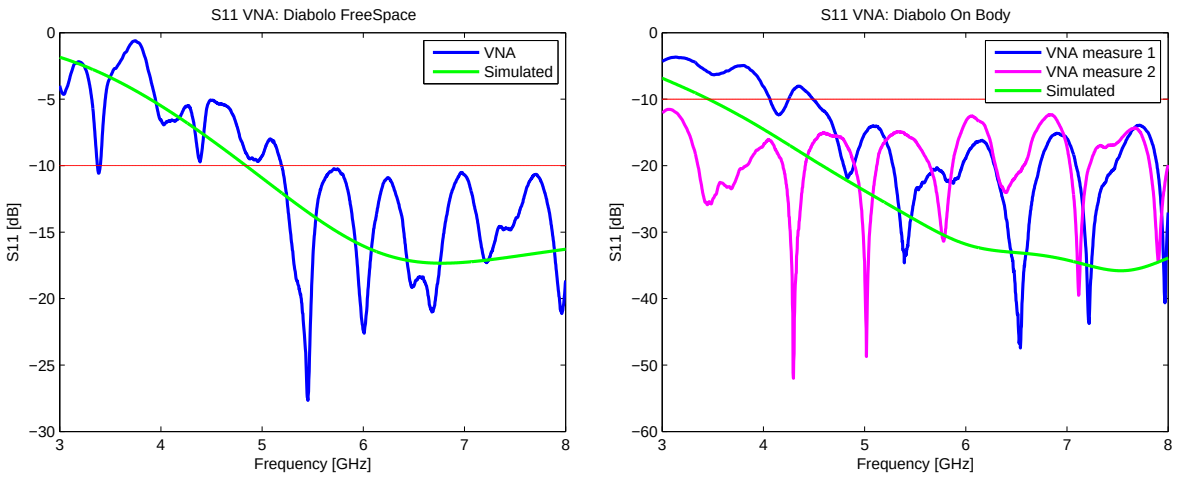

a) b)

Figure 4.19: S_{11} parameters measured in a VNA. *(a) Free Space.(b) On body (Hand).*

This S_{11} parameter explains the losses of the antennas, but does not prove that the antennas are indeed radiating. They could be turning all the power into heating themselves. To check the transmission, the S_{21} between the volcano and the diabolo antenna was measured with the VNA. This will not give us any cuantitative result, but will help us to check if the antennas are radiating. Figure 4.20 shows the S_{21} parameter in free space when one antenna is placed 20 cm away from the other.Figure 4.20 (a) displays the co-polarization with an average value of -34 dB, which is around 20 dB higher than the cross polarization (around -50 dB) displayed in figure 4.20 (b). This validates the linear polarization of the antennas. The initial valley at 3.2 GHz is due to the high losses in both antennas, with both S_{11} parameters above -10 dB. After that, the S_{21} increases up to -31 dB due to the low losses of the volcano. At 7 GHz, the high losses of the volcano are compensated with the low losses of the diabolo, providing a S_{21} relatively constant.

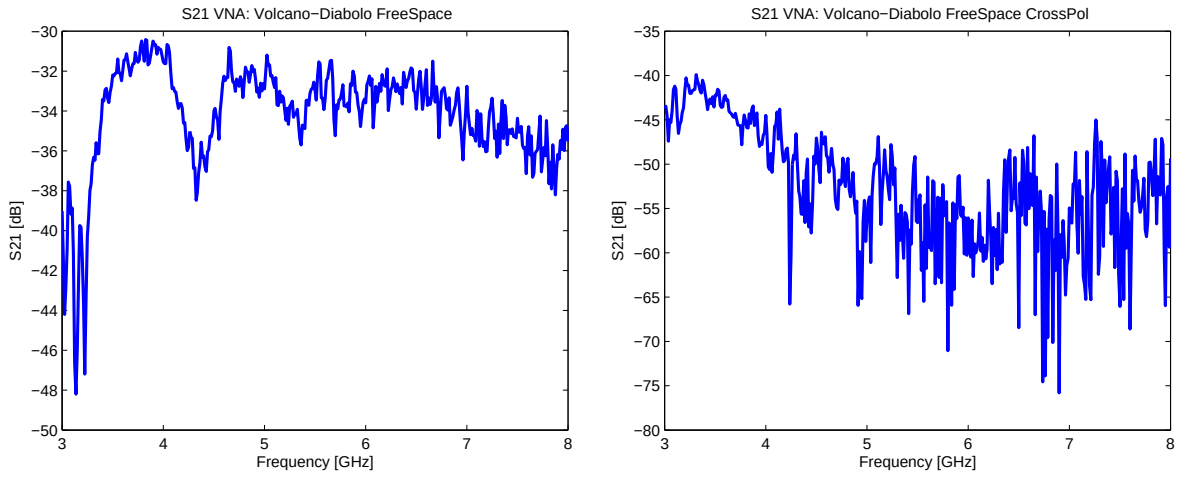

a) b)

Figure 4.20: S_{21} (Volcano-Diabolo) parameters measured in a VNA. *(a) Co-Polarization. (b) Cross-Polarization.*

Chapter 5

LINK LOSS

This chapter is dedicated to the study of the link loss in WBAN.

5.1 Deterministic Link Loss Model in WBAN scenario

The purpose of this research is to check if the model for the propagation over an elipse (around human waist) of a narrowband signal can be related with the propagation of a wide band signal.In this case, UWB range has been studied instead of the 2.45 GHz. As explained in [37], the paths of both sides of the ellipse will create constructive and destructive interference depending on the position of the antennas. The analytical model proposed for a 2.6 GHZ narrowband signal is presented in the equation (5.1), where G_{tx} and G_{rx} are the transmitter and reciever antenna Gain, Lc and Lac are the attenuation of the E-field clock-wise and anti-clock-wise which are calculated as (5.2), and $\mathbf{p}$ and d_n are the elipse perimeter and the minimun distance from the transmiter to the reciever antenna, calculated with (5.3), where a and b are the major and minor axes of the ellipse.

$$LL_n|dB = -10log_{10}\left[\frac{G_{RX}G_{TX}\lambda^2}{4\pi^2}\left(\left|\frac{e^{-L_{cn}}}{d_n}e^{-jkd_n}+\frac{e^{-L_{acn}}}{p-d_n}e^{-jk(p-d_n)}\right|\right)^2\right] \tag{5.1}$$

$$L(\varphi_1,\varphi_2) = \frac{(k)^{1/3}}{2}\left(\frac{3\pi ab}{4}\right)^{2/3}e^{\frac{j\pi}{6}}\cdot\int_{\varphi_2}^{\varphi_1}\frac{ab}{\sqrt{[a^4cos^2\phi+b^4sin^2\phi]\,[a^2cos^2\phi+b^2sin^2\phi]}}d\varphi \tag{5.2}$$

$$arc = ab\int_{\phi_2}^{\phi_1}\frac{(a^4cos^2\phi+b^4sin^2\phi)^{1/2}}{(a^2cos^2\phi+b^2sin^2\phi)^{3/2}}d\phi \tag{5.3}$$

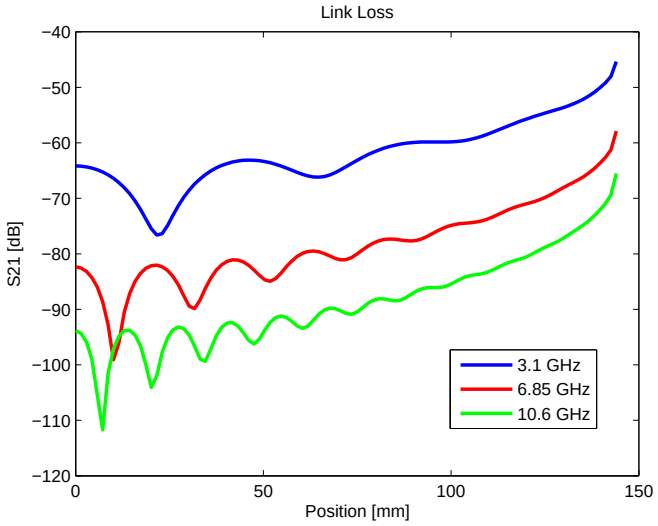

Figure 5.1: *Deterministic calculation for the link loss model around a human waist.*

The figure 5.1 shows the result for the path gain for three different frequencies. The X-axis are the position in mm along the major axis of the elipse. It is seen that the higher the frequency the higher the losses. This is a normal behaviour since the attenuation, reflection, scattering and other effects are more noticeable in higher frequencies. Also the number of constructive/destructive interferences is bigger in higher frequencies since the wavelength is smaller.

5.2 Statistical Link Loss Model in Free Space

Using the two antennas that have been designed, a study of the statistical link loss model in an indoor enviroment with LOS have been done with the results extracted from the VNA. The data was taken for 10 positions for the antennas, shown in table 5.1. Here, the S_{21} parameter have been considered as the PL (dB) according to the formula (5.4), where the PL has been taken as the average over the entire frequency band.

$$PL = -|S_{21}| = PL_{0dB} + 10n \cdot log_{10}(\frac{d}{d_0}) \tag{5.4}$$

The Fraunhoffer boundary taken as $2D^2/\lambda$ [7] states the far field region, with D the diameter of the antenna. For D = 45 mm and f = 10.6 GHz, the Fraunhoffer distance results in $d_F = 13.78$ cm. Since the positions must be in the far field region, by taking $d_0 = 20$ cm as the reference distance and $PL_{0dB} = 34.13$ dB as the Path Loss reference, the path loss exponent n is obtained.

For this case, n=1.98, which verifies the free space situation, that is n = 2. Figure 5.2 shows how the path loss increases with the distance.

Path Loss [dB]	Distance [cm]
34.13	20
36.08	25
38	30
39.11	35
40.24	40
41.12	45
41.32	50
42.3	55
43.38	60
44.08	65

Tabla 5.1: Values obtained with the VNA

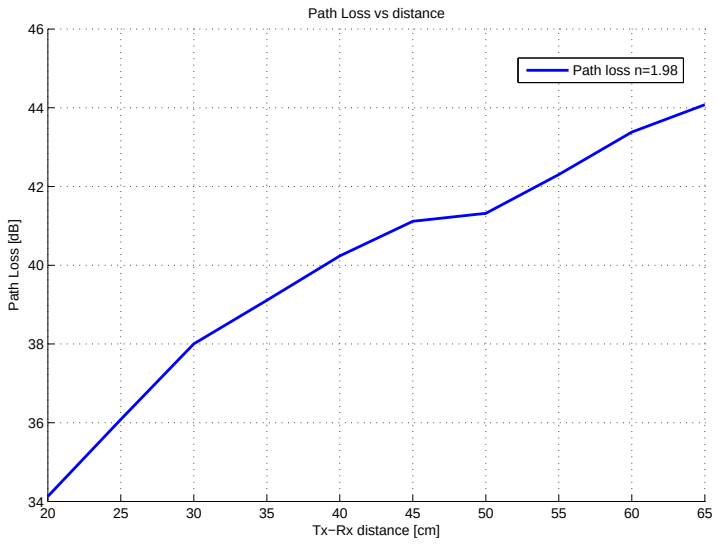

Figure 5.2: *Statistical calculation for the link loss model in an indoor environment with LOS.*

Chapter 6

CONCLUSION

In this project two 3D UWB antennas have been designed to be used in a WBAN scenario: a volcano antenna (27x45x45 mm) and a diabolo shaped antenna (15x17x17 mm). In both of them the matching within the UWB range (3.1 GHz - 10.6 GHz) is achieved.

The design of the antennas has been made by using the SEMCAD X software tool to perform the simulations. Both situations, on free space and with the presence of a homogeneous human phantom, have been simulated for each antenna. Afterwards, the results have been checked with a vector network analyzer.

The radiattion patterns follow an omnidirectional distribution in the perpendicular polarization in all the frequency range. The volcano antenna presents a more stable S_{11} parameter in presence of a human body. On the other hand, the diabolo shaped antenna presents a S_{11} more sensitive to the human body. This is due to the smaller size of the ground plane.

During the measurement process, several difficulties appeared. First, the metal used to manufacture the antenna (steel) presented soldering problems, since the tin did not stick properly to the metal. Secondly the conductivity of the steel was too bad to assume a PEC. As a result it showed a lot reflections. To solve this the antenna was covered with copper, achieving a better matching. Another issue was the cable effects due to the small size of the antennas. This problem was partially solved by adding a long (14 cm), thin cable between the feeding point and the SMA connector.

Chapter 7

FUTURE WORK

For further researches in this project, a new manufacture of the antennas can be made in order to improve its conductivity. The company Shapeways offers other materials like silver which not only has higher conductivity but a higher level of detail and smoothness in the piece is offered in the manufacturing process (Min detail steel: 1 mm, min detail silver: 0.3 mm [26]). Another (and probably cheaper) method is to cover the antenna with copper by electroplating. This method is often used to cover a metal that lacks a property with another metal that has it.

One of the limitations of the project was the measurement technique. In this case a Vector Network Analyser was used with an SMA connector. The problem of this method is that the cable used to connet the VNA and the antenna affects in the results. The smaller the size of the antenna the bigger the cable effect. For further investigations another method for feeding the antenna should be studied in order to decrease this cable effect and have more reliable results.

Proper measurements of the S_{11} and S_{21} on the body would be also another step in the project. The use of a container with human shape filled with liquid with dielectric properties similar to the skin can be used for this purpose. The use of an anechoic chamber to measure the variation of the radiation pattern with frequency would be also desirable.

Also other techniques for miniaturization like the use of shorting pins or the use of dielectric materials covering the antenna should be studied more in detail. In this project some simulations with shorting pins were made without usefull results.

Another goal is to find a suitable application for this antennas in a WBAN system.

Bibliography

[1] H. Sjöland, P. Nilsson, and R. Chandra. J. Neves Rodrigues A.J.Johansson. A receiver architecture for devices in wban. *Emerging and selected topic in circuits and systems*, 2:82–95, March 2012.

[2] Jamil. Y Khan and Mehmet R. Yuce. Wban for medical applications. *School of electrical engineering ang computer science, University of New Castle, Australia.*, Feb 2006.

[3] http://www.antenna-theory.com/basics/directivity.php.

[4] Karu P. Esselle Tharaka Dissanayake. How do you select the best antenna for you ultra-wideband system. *Workshop on applications of radio science.La Trobe University, Victoria Austalia.*, Feb 2006.

[5] Anders J. Johansson Rohit Chandra. An elliptical analytic link loss model for wireless propagation around the human torso. *6th European Conference on Antennas and Propagation (EUCAP)*, pages 3121–3124, Marzo 2012.

[6] Ramjee Prasad Homayoun Nikookar. *Introduction to UWB for Wireless Communication.* Springer., first edition, 2009.

[7] B. Allen. *Ultra-wideband Antennas and Propagation.* John Wiley&sons.., West Sussex, England, first edition, 2007.

[8] Gerald D. Rogerson C.Roberto Aiello. Ultra-wideband wireless systems. *IEEE Microwave magazine*, first,1527-3342:36–47, june 2003.

[9] EC Committee. The harmonised conditions for devices using ultra-wideband technology in bands below 10.6 ghz. *ECC Decisions*, (06)04, march 2006.

[10] Sheng-Yi Huang YD Chen Cheng-Hung Lin Guan-Yu Chen, Jwo-Shiun Sun. Characteristics of uwb antenna and wave propagation. *IEEE International Symposium on intelligent signal processing and communiction systems*, 0-7803-9266-3:713–716, december 2005.

[11] B. Sreedevi. Emi issues in uwb systems. *IEEE 9th Conference on Electromagnetic interference and compatibility*, pages 417–424, february 2006.

[12] David Puente-Cong Ling Xiaodong Chen Daniel Valderas, Juan Ignacio Sancho. *Ultrawideband antennas, design and applications.* Imperial College Press, London, UK, first edition, 2011.

[13] A.Rajkotia S.A.H.Mohammadian. Characterization of uwb transmit-receive antenna system. *IEEE Conference on UWB systems and technologies*, pages 157–161, november 2003.

[14] J.McCorkle. Uwb: Gigabit wireless communications for battery operated consumer applications. *IEEE Symposium on VLSI circuits*, pages 6–9, june 2005.

[15] Zhi Ning Chen. Uwb antennas: design and application. *IEEE International conference on information, communications and signal processing*, 1-4244-0983-7, december 2007.

[16] R Yuce Jamil Y. Khan. Wireless body area networks, technology, implementation and applications. 2012.

[17] Xianming Qing Zhi Ning Chen, Terence S. P. See. Small ground-independent planar uwb antenna. *IEEE International Symposium of Antennas and Propagation Society.*, pages 1635–1638, July 2006.

[18] Constantine A. Balananis. *Modern Antenna Handbook.* John Wiley&sons., West Sussex, England, first edition, 2008.

[19] http://www.phys.hawaii.edu/~anita/new/papers/militaryHandbook/radiapat.pdf.

[20] Johnna Powell. Antenna design for ultra wideband radio. *Masther of science in Electrical engineering at the MIT.*, May 2004.

[21] Chung-Chou Shen Jin-Shyan Lee, Yu-Wei Su. A comparative study of wireless protocols: Bluetooth, uwb; zigbee and wifi. *IEEE The 33rd Annual conference of the IEEE Industrial Electronics Society (IECON)*, pages 46–51, November 2007.

[22] R.Sauleau K.Ito N.Chahat, M.Zhadobov. A compact uwb antenna for on-body applications. *IEEE Transactions on antenna and propagation*, 59(4):1123–1131, April 2011.

[23] Han Yu-nan Zhang Chun-Qing, Wang Jun-Hong. Coupled planar dipole uwb antenna design for wearable computer. *IEEE International conference on microwave and milimeter wave technology*, pages 1–4, April 2007.

[24] X.Hu C.G.Parini-P.S.Hall A. Alomainy, Y.Hao. Uwb on-body radio propagation and system modelling for wireless body-centric networks. *IEEE Proceedings communications*, 153(1):107–114, February 2006.

[25] A.Yarovoy A. Vorobyov. Human body impact on uwb antenna radiation. *Progress in electromagnetics research M.*, 22:259–269, 2012.

[26] http://www.shapeways.com/materials/material-options.

[27] http://www.speag.com/products/semcad/solutions/.

[28] http://www.pdc.kth.se/training/2002/SummerSchool/CourseWork/FDTD/index.pdf.

[29] http://www.eecs.wsu.edu/~schneidj/ufdtd/chap3.pdf.

[30] http://www.optiwave.com/pdf/literature/MS535510.pdf.

[31] http://niremf.ifac.cnr.it/tissprop/htmlclie/uniquery.php?func=atsffun&freq=6.85e9&outform=tabl&tisname=on&conduct=on&permitt=on&losstan=on&wavelen=on&pendept=on.

[32] Takehiko Kobayashi Takuya Taniguchi. An omnidirectional and low-vswr antenna for the fcc-approved uwb frequency band. *IEEE antennas and propagation society international symposium*, 3:460–463, june 2003.

[33] john D. Kraus. *Antennas for all applications.* Mc Graw Hill., Avenue of americas, NY 10020, third edition, 2002.

[34] G.P. Gao, X.X. Yang, J.S. Zhang, and J.X. Xiao. A printed volcano smoke antenna for uwb and wlan communications. *Progress in electromagnetics research M.*, 4:55–61, 2008.

[35] K. Sato K. Koshiji F. Koshiji, T. Eguchi. Proposal and investigation of a flat type small volcano smoke antenna. *International Symposium on antennas and propagation*, pages 1–6, 2006.

[36] K.P. Ray N.P. Agrawall, G. Kumar. Wide-band planar monopole antennas. *IEEE Transactions on antennas and propagation*, 46:294–295, Febreary 1998.

[37] Anders J. Johansson Rohit Chandra. An elliptical analytic link loss model for wireless propagation around the human torso. *6th European Conference on Antennas and Propagation (EUCAP)*, pages 3121–3124, Marzo 2012.